Universidad
Tecnológica
de Pereira

MASTER'S PROGRAM IN ELECTRICAL ENGINEERING

MASTER THESIS

CONVEX OPTIMIZATION FOR STABILITY ANALYSIS IN DC MICROGRIDS

Vanesa Londoño Marín

Supervisors:
Dr.Alejandro GARCÉS RUIZ

Dr.Walter GIL GONZÁLEZ

December 14 2020

Dedicado a
mis padres.

Abstract

Direct current (DC) microgrids are a technology that promises advantages such as efficiency and reliability, for integrating renewable energy and storage devices. However, DC microgrids present stability problems, since it requires power electronic converters. Therefore, it is important to develop stability analysis tools that can be general and applicable to any configuration type. The eigenvalues small- signal method is applied to identify with parameters that affect more the stability of the system, where the sensibility analysis improves the oscillations of the microgrid. This thesis employs convex optimization models to determine stability conditions in the sense of Lyapunov in DC microgrids. The use of convex optimization methods allows a systematic approach to the construction of Lyapunov functions in systems with different configurations. These functions can also be used to estimate regions of attraction that are principal for the calibration of the parameters value analysis selecting the correct steady-stead performance.

Acknowledgments

I would like to offer my special thanks to my supervisor Professor Alejandro Graces and Walter Gil for all their patient guidance, knowledge, and valuable support in my master's thesis.

I would also like to extend my thanks to my family for all their unconditional support.

Contents

Chapter 1

Introduction

1.1 Problem Description

Microgrids are known to be one of the biggest revolutions in power systems, due to the incorporation of new technologies as renewable energy. These systems are integrated with synchronous generator and energy storage by converters implemented to mitigate the stochastic variation of renewable energy. However, microgrids are intrinsically nonlinear as a result of the presence of power converters DC/AC, which implies difficult analysis. Therefore, it is necessary to apply linear control [Diaz et al., 2015] allowing the microgrid to maintain their stability and provide the required power to the grid. The majority of development research about DC microgrids is focused on the form that the energy flow must be coordinated between distributed generation, energy storage location, and load. To optimize the stability of the output variable as well as energy-saving efficiency [Zhang et al., 2013].

Stability analysis in microgrids is complex resulting in the way in which it is connected. For instance, they can work grid-connected or island mode, although it requires auxiliary services, frequency, and reactive control. However, DC microgrids do not need frequency and reactive power control [Che et al., 2015]. Stability analysis can not be limited to the stability of the elements separately, instead, it is necessary to study the dynamic interactions of the system. Besides, it is required to linearize the system to apply theoretical small-signal stability methods, where the sensibility analysis is employed to identify the parameters that most affect microgrid's stability.

Named after Russian mathematician Mikhailovich Lyapunov, Lyapunov theory is an adequate method to analyze stability in microgrids; Otherwise, it is a difficult problem to find Lyapunov functions even in small systems. In numerous cases, the knowledge of the physical systems is used to encounter possibles Lyapunov functions. For this reason, it is necessary to develop systematic ways

to find Lyapunov functions that guarantee stability and estimate the region of attraction. One way to find these Lyapunov functions is through the use of optimization models, among which polynomial optimization, the sum of quadratic polynomials [Blekherman et al., 2012], matrix inequalities [Boyd et al., 1994] and Lasserre hierarchies [Cominetti et al., 2012], among others. All these models can be solved under the paradigm of convex optimization. However, the solution of these models can be computationally expensive. For this reason, it is predominant to include expert knowledge in a particular model.

1.2 Motivation

In recent years, DC microgrid distribution systems have become an attractive systems due to their natural interface with renewable energy sources, electric loads, and energy storage systems [Kumar et al., 2017]. However, DC microgrids are integrated with the new energy through power electronic converters and controlled to maintain constant power. These power loads can introduce a negative resistance generating stability problems. Questions such as how to build corresponding mathematical models of the system, and how to develop methods for stability analysis, which are different from the DC microgrids methodologies, are required for the integration of these technologies in grid-connected and islanded topology.

The diversification of Colombia's transition system is required to increase power transmission capacity, where the generation depends mainly on hydro resources (80.35% of generation), demonstrating the potential for generating electricity by using renewable energy [xm, 2020]. Microgrids stability analysis is necessary to guarantee efficiency and reliability. Therefore, stability analysis is required to include the primary control effect, due to microgrids are being controlled by power electronic converters. In [Garces, 2020] analysed the classification of the stability, developing a different approach compared to conventional power systems; It reveals that fast time constant and low values of droop control are required to assurance stability. This study was developed for island microgrids; when those devices are directly connected to the grid, optimal control is required to transfer the power from the energy sources to the AC generator.

On the other hand, Convex optimization has great advantages in all of its methods since the problem is solved efficiently. The methods to solve can be programmed in different computational tools providing an answer to the problem presented. Also, it has theoretical advantages, as each of its methods presents an interesting formulation, and it can be applied to generate Lyapunov functions in a dynamic time. This allows estimating the region of attraction in microgrids, and demonstrate convergence and global solution.

While showing promising results in the residential and commercial sectors,

DC microgrid distribution systems still need further analysis to ensure long-term stability and safety. Control strategies are mandatory to conjoin the power electronic converters with the grid, establishing the equilibrium point for analysis such as stability and optimal operation. Transforming the power flow equations into an optimization model, using convex optimization, is possible to determine its convergence and uniqueness of the solution. Therefore, a precise but simple model of the DC microgrid is required.

1.3 State of the art

Studies in DC distribution systems and DC microgrids show the feasibility of implementing DC distribution in different aspects and applications in DC power systems protection and stability. However, AC power systems predominant in distribution, and the major reason is the transformers that give a simple process to step up the voltage. Currently, with power electronics, which made DC regulation a simple task, the efficiency is increased since it does not need many conversion stages, which add inefficiencies as the majority of consumer loads are DC supplied like industrial applications [Dastgeer et al., 2019].

One of the best benefits of DC microgrids is the feasibility of static storage integration, and some of the renewable energy sources are naively DC. They can be locally controlled and solve the problems with blackout disconnecting the grid and continue providing energy like an island mode. To design a DC distribution system is major to choose simplified models that express real behavior based on system operation and control. The authors in [Elsayed et al., 2015] also talk about the standard defines in DC power distribution that is key points to know about the main guiding lines for the installation of DC technologies.

Distributed energy resources (DERs) as small hydro-power plants (SHP) mitigate the problem of the stochastic variation of solar radiation and temperature by implementing a permanent magnet synchronous generator (PMSG) connected to a DC microgrid via a voltage source converter (VSC). In general, the VSC model incorporates the AC side model and DC side with the coupling equations. Where the AC model represents the mechanical energy in the hydraulic turbine to electrical power, and the DC model composes a dynamic model of the DC link. The controller for the SHP model based on the passivity theory guarantees the stability of the system [Gil-González et al., 2020b].

DC microgrids are integrated through power electronic converters and controlled to maintain constant power. These power loads can introduce a negative resistance generating stability problems. Hence, several methods have been developed to ensure stability for DC microgrids; which include transient stability, small-signal stability, and grid-connected inverters analysis. Where the dynamical model of the system is vital since it is required to obtain a strong

model and high simulation efficiency. Therefore, some authors use linearized equations to develop a steady-state model [Wang et al., 2020][Liu et al., 2015]. While others apply a gradient system generated by a strongly convex function, thus, the stability analysis is simplified to a series of convex optimization problems [Garcés, 2019]. The cause of instability can be found by utilizing the Lyapunov and eigenvalues method, that employ the sensitivity analysis to determine the effect of DC microgrid parameters on the dominant poles [Shakerighadi et al., 2018].

Linear matrix inequalities (LMIs) generate quadratic functions that are considered Lyapunov functions in linear systems to optimization problems, with the higher level providing on the application. On the other hand, DC microgrids are composed of storage and constant power loads (CPLs) that are nonlinear and may cause instability associating optimal problems control with CPL and voltage stability. Authors in [Liu et al., 2017], used the control Lyapunov function to model asymptotic control laws with robust stability. Thus, it has been found that convex optimization problems robust stability provided polytopic uncertainties on system matrices.

Table 1.1 contains in a visual scheme the portion that is considered in the articles cited above, evidencing the network topology that is proposed, for this application is not complete study in those papers. Also, it is compared and presented with the list of topics described in the different chapters of this thesis, where robust optimization is fully included.

Table 1.1: Various considerations of papers about thesis topics.

Reference	[Dastgeer et al., 2019]	[Elsayed et al., 2015]	[Gil-González et al., 2020b]	[Wang et al., 2020]	[Liu et al., 2015]	[Garcés, 2019]	[Shakerighadi et al., 2018]	[Liu et al., 2017]	Thesis
Network topology	◓	◓	◓	◔	◔	◓	◔	◔	●
Control desing DC	○	○	◔	◓	◓	◓	◓	◓	●
Stability analysis	○	○	◔	●	●	●	◓	◓	●
Convex Optimization	○	○	○	○	○	●	○	●	●
Robust Optimization	○	○	○	○	○	○	○	◔	●

○ means not considered; ◔ means partially considered;
● means fully considered; ◓ means relatively considered.

1.4 Organization

In this paper, Section II introduces a comprehensive definition of the control schemes for DC microgrid, as the configuration with the steady-state model and the blocks simulation. Section III explains the small-signal analysis formulated by linearizing the dynamical model of the system for the analysis of eigenvalues and modes of oscillations applying Lyapunov theory. Section IV focuses on the validation and robustness of the proposed model thought convex optimization. Section V presented the conclusions of this thesis.

The results are partially organized for each chapter, with an additional summary at the end of the chapters. In that order of ideas, Chapter II demonstrates the correct formulation of control for the proposed DC microgrid since it is possible to show, with the simulation of blocks, that dynamical equations are correctly formulated and can be applying for n converters. The stability analysis in Chapter III demonstrates the appropriate and robust behavior of the parameters in the system since the micro DC network is stable, despite the different disturbances. Additionally, the damping ratio results improves the stability of the DC microgrid due to can be proved that Newton's method is a satisfactory technique

to find the value with small error, as well as the steady-state equations correctly modeling the system.

Chapter 2

Microgrid configuration

Power-sharing accuracy is developed to reduce line loss and improve the overall efficiency of the direct-current (DC) microgrids. At the same time, electronic converters are essential to integrate into renewable energy with local alternating-current (AC) generators. Moreover, the system's stability can be improved with the correct state-space model, where a block simulation is required to guarantee the correct formulation. This chapter provides a comprehensive definition of the control for DC microgrid, and the equations for the model design.

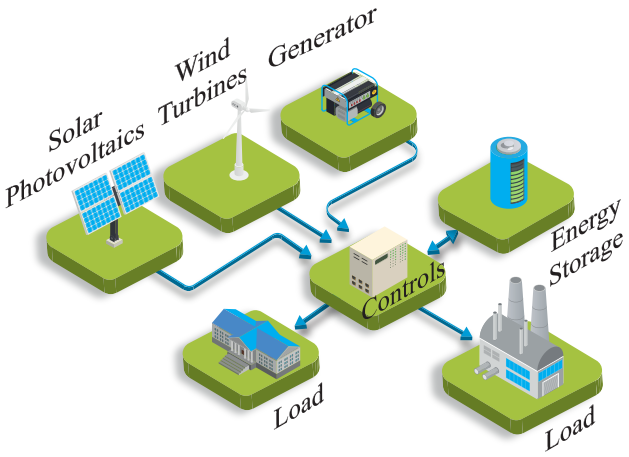

Figure 2.1: Scheme of a DC microgrid.

The concept of a microgrid is introduced as a low voltage energy distribution that posses its energy resources. The structure is formed by the synchronous generators, a battery energy storage system, a distributed generator, and cus-

tomer loads, as shown in Figure 2.1. Microgrids can operate in grid-connected or island mode, and they are represented as controllable loads. In island mode, it includes distributed generation (DG) that is mainly shaped with solar and wind renewable energy sources [dos Santos Neto et al., 2020]. Instead, DC microgrids with DG posses a stochastic variation, and need a synchronous generator to improve the power stability .

Table 2.1 shows all the symbols used to describe the system.

Table 2.1: Description of the used symbols

State variables	
V_{DC_i}	DC voltage
I_{k_i}	Circuit current
I_{d_i}	Grid current
V_{load}	Load voltage
$I_{d\text{ref}_i}$	Grid reference current
$V_{d\text{ref}_i}$	Grid reference voltage
P_{of_i}	Reference power
Parameters	
C_c	Common capacitor
R_c	Load
C_{DC_i}	DC capacitor
L_{DC_i}	DC inductance
R_{DC_i}	DC resistance
R_{grid_i}	Filter resistance
L_{grid_i}	Filter inductance
Inputs	
V_{grid_i}	Grid voltage
V_{ref_i}	Reference voltage
P_i	Grid Power

2.1 Design of the control

The DC microgrid illustrated in Figure 2.2 consists of a single node that can have as many converters as is necessary for the operation feeding. It considers a generator, a converter, and a linear load in parallel with a capacitor. Park reference frame transformations have been used to simplify the connection between the control system and power electronics systems reducing generator variables. Therefore, the active power can be managed independently by controlling the $dq0$ components while considering voltage source converters (VSCs) as the interfacing devices [Manias, 2016]. However, the generator information is keeping in mind without using the phase-locked loop (PLL), since the analysis is based on the DC side, assuming the PLL works perfectly, and the power

given by the utility grid can be garanteed with an external control described in [Gil-González et al., 2020b]. For this application, the park's transformation power-invariant is used.

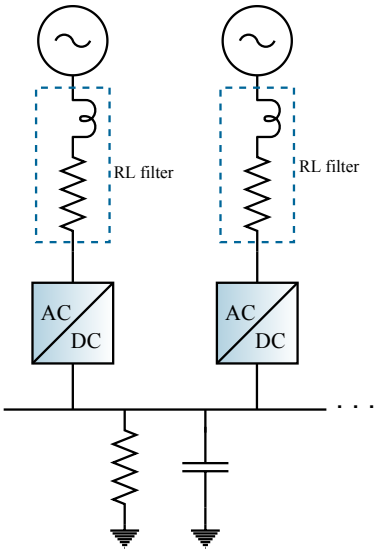

Figure 2.2: Block diagram of a microgrid under study.

2.1.1 AC generator

DC microgrids operate in grid-connected or island mode, thus various AC-generating sources can be implemented depending on the operating mode. When the microgrid is disconnected from the utility grid or in island mode, the AC part is replaced by a diesel plant or a hydro-power plant (SHP), among others. For example, the SHP consists of a penstock, a hydro turbine, a governor system, and a generator. The power output is control by the generator through the hydraulic turbine's water flow [Gil-González et al., 2020a]. The permanent magnet synchronous generator (PMSG) transforms the mechanical energy in the hydraulic turbine to electric power. It is Assumed that the SHP's control posses a correct operation giving the required output power. Thus, VSC regulates the electrical power by keeping the DC-link voltage V_{DC} constant.

2.1.2 The voltage source converter

Power electronic converters are required to integrate local loads and distributed sources into the grid. Figure 2.3 shows the topology of a two-level VSC connected to the microgrid through an RL filter. The DC circuit is represented with a capacitor as an energy storage device. The VSC self-commutating switches, as gate turn-off thyristors (GTOs), insulated gate bipolar transistors (IGBTs),

or gate controlled thyristors (IGCTs), can be turned on or off in a controlled manner [Kalitjuka, 2011]. VSCs can control the active power independently the switching by a three-phase Pulse-Width Modulated (PWM) converter. The switching of the IGBTs values follows a PWM pattern, allowing simultaneous adjustment of the amplitude and phase angle of the converter output voltage with constant DC voltage.

By applying Kirchoff's Voltage law in Figure 2.3, it is possible to obtain the relationship among the VSC input voltages V_{abc}, the grid voltages E_{abc} , the output currents $_{Iabc}$, as follows

$$E_{abc} = L_{\text{grid}} \frac{d}{dt} I_{abc} + V_{abc} + R_{\text{grid}} I_{abc}. \tag{2.1}$$

Where L_{grid} is the filter inductance and R_{grid} is the filter resistance.

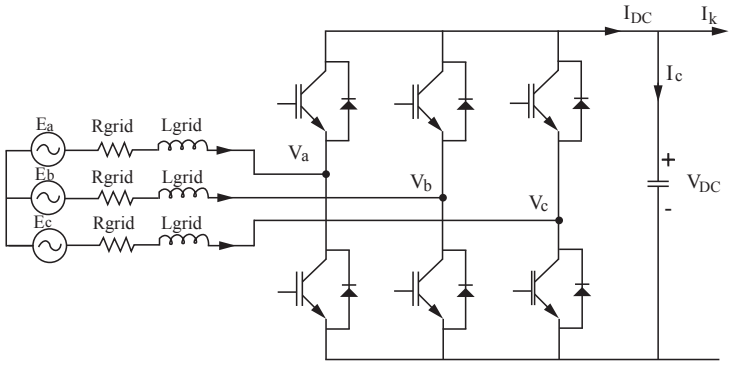

Figure 2.3: Schematic representation of the VSC system.

Control of the grid-connected VSC is often based on current methods, which is designed in a grid voltage-oriented synchronously rotating reference frame well-known dq reference frame. The most common controllers applied to the VSC are the proportional-integral (PI) and linear control techniques. PLL is required for the coordinate transformation where the phase angle is calculated by employing PLL and allows space vector based controllers to be implemented [Wang et al., 2017]. A properly adjusted synchronous controller allows the AC variables have a behavior as DC variables [Teodorescu et al., 2011].

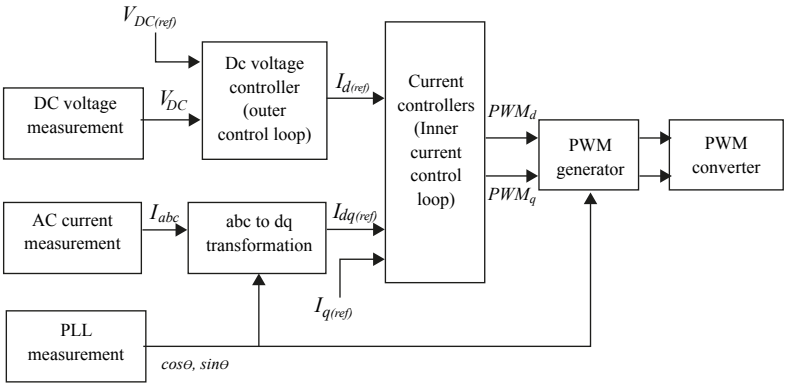

Figure 2.4: Vector control strategy for the VSC.

2.1.3 Park transformation

Park transformation is used to transform the abc three-phase components to the synchronous reference frame. The power invariant $dq0$ transform is employed and expressed as

$$\begin{bmatrix} x_d \\ x_q \\ x_0 \end{bmatrix} = [x_r], \tag{2.2}$$

$$[x_r] = [T] \cdot [x], \tag{2.3}$$

$$[x_r] = [T] \cdot \begin{bmatrix} x_a \\ x_b \\ x_c \end{bmatrix}. \tag{2.4}$$

This transformation can be applied for currents or voltage power flow in a three-phase system, with the rotating matrix $[T]$.

$$[T] = \sqrt{\frac{2}{3}} \begin{bmatrix} \cos\theta & \cos(\theta - \frac{2\pi}{3}) & \cos(\theta + \frac{2\pi}{3}) \\ \operatorname{sen}\theta & \operatorname{sen}(\theta - \frac{2\pi}{3}) & \operatorname{sen}(\theta + \frac{2\pi}{3}) \\ \frac{1}{\sqrt{2}} & \frac{1}{\sqrt{2}} & \frac{1}{\sqrt{2}}, \end{bmatrix}$$

the power invariant Park's transformation is orthogonal uniformly-scaled, which fulfills, $[T]^{-1} = [T]^{\top}$ meaning the power in both reference frames is equal $P_{abc} = P_{dq0}$.

The relationship between the abc frame and $dq0$ frame may be expressed as (2.5).

$$[V_{dq0}] = \underbrace{[T]}_{wt} [V_{abc}], \tag{2.5}$$

$$V_d = \cos\theta\ V_a + \cos\theta - \frac{2\pi}{3}\ V_b + \cos\theta + \frac{2\pi}{3} V_c,$$
$$V_q = \operatorname{sen}\theta\ V_a + \operatorname{sen}\theta - \frac{2\pi}{3}\ V_b + \operatorname{sen}\theta + \frac{2\pi}{3} V_c. \tag{2.6}$$

where V_d and V_q are the converter terminal voltages in dq frame.

Power calculation in the synchronous reference frame is defined as [Peng and Lai, 1996].

$$\begin{aligned} S &= P + jQ, \\ S_{dq} &= V_{dq} I_{dq^*}, \\ V_{dq} &= V_d + jV_q, \\ I_{dq} &= I_d + jI_q, \\ S_{dq} &= \underbrace{V_d I_d + V_q I_q}_{P} + j\underbrace{\left(V_q I_d - V_d I_q\right)}_{Q}. \end{aligned}$$

Hence, active power in Park transformation in two-phases (dq) based on last equation can be expressed as (2.7).

$$P_{AC} = V_d I_d + V_q I_q, \tag{2.7}$$

typically, the PLL is designed to align it to the q voltage, hence, $V_q = 0$ and the active power can simplify, as follows

$$P_{AC} = V_d I_d, \tag{2.8}$$

where $V_d = V_{\text{grid}}$

$$P_{AC} = V_{\text{grid}} I_d. \tag{2.9}$$

2.1.4 DC Circuit

In this study, we consider two converter-based DC microgrid to facilitate the analysis; nevertheless, the equations are first explained for one converter and later they will be expressed in a general way. The DC microgrid dynamics can be expressed as a state-space model.

Assuming that the electronic components have no losses, the power on the AC side is equal with the power that is transferred from the DC side;

$$P_{AC} = P_{DC}. \tag{2.10}$$

From (2.7) we have that:

$$V_{\text{grid}} I_d = V_{DC} I_{DC}. \tag{2.11}$$

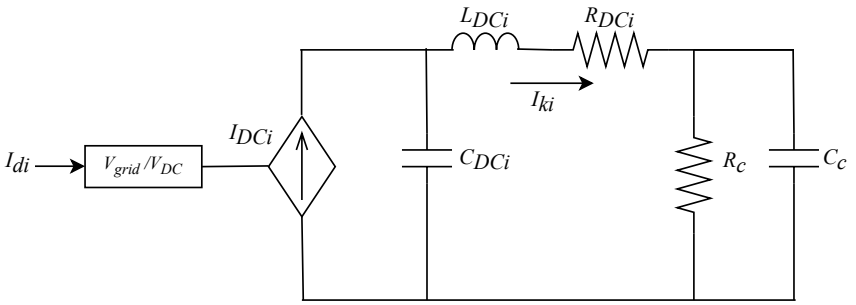

Figure 2.5: Diagram of the DC side.

Applying Kirchhoff's current and voltage laws, and (2.11), the following equations are found:

$$\begin{aligned} C_{DC_1}\dot{x}_1 &= \frac{V_{\text{grid}} - x_3}{x_1} - x_2, \\ \dot{x}_2 &= x_1 - R_{DC_1}x_2 - x_7, \\ C_c\dot{x}_7 &= x_2 - \frac{x_7}{R_c}, \end{aligned}$$

where x_1, x_2, and x_7 are the state variables defined as follows:

$$\begin{aligned} x_1 &= V_{DC1}, \\ x_2 &= I_{k1}, \\ x_7 &= V_{\text{load}}. \end{aligned}$$

2.1.5 Inner Loop

The inner loop can control the power between the DC-link and the grid, the constant quantities are necessary to design the control scheme. For that reason the mathematical model of the three-phase inverter in abc coordinates is transformed into a mathematical model of the three-phase inverter in $dq0$. Consequently, in (2.12) is given in $dq0$ reference, where w is the system frequency in rad/s [Yazdani and Iravani, 2010].

$$\begin{bmatrix} E_d \\ E_q \end{bmatrix} = L_{\text{grid}}\frac{d}{dt}\begin{bmatrix} I_d \\ I_q \end{bmatrix} + wL_{\text{grid}}\begin{bmatrix} 0 & -1 \\ -1 & 0 \end{bmatrix}\begin{bmatrix} I_d \\ I_q \end{bmatrix} + R_{\text{grid}}\begin{bmatrix} I_d \\ I_q \end{bmatrix} + \begin{bmatrix} V_d \\ V_q \end{bmatrix} \tag{2.12}$$

Expanding, the voltage equations are

$$\begin{aligned} E_d &= L_{\text{grid}}\frac{d}{dt}I_d - wL_{\text{grid}}I_q + V_d + R_{\text{grid}}I_d, \\ E_q &= L_{\text{grid}}\frac{d}{dt}I_q + wL_{\text{grid}}I_d + V_q + R_{\text{grid}}I_d. \end{aligned} \tag{2.13}$$

To control the currents applying PI controllers the equation is written as follow

$$U(s) = \left(K_{pi} + \frac{K_{iI}}{s}\right) F(s), \tag{2.14}$$

where $F(s) = I_{d_i(\text{ref})} - I_{d_i}$.

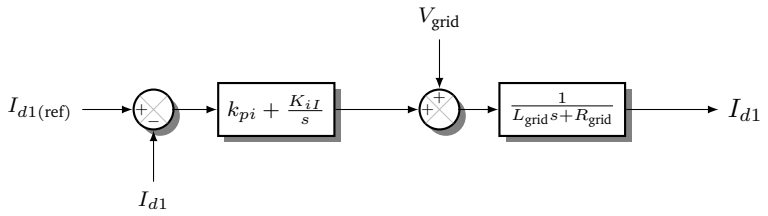

Figure 2.6: Control block diagram for the Inner Loop.

Figure 2.6 presents the control structure to regulate I_{d_i} as $I_{d_i(\text{ref})}$.

The transfer function in Figure 2.6 is given by:

$$\frac{Y(s)}{X(s)} = \frac{G(s)}{1 + G(s)H(s)}, \tag{2.15}$$

where $X(s)$ is the reference input, $Y(s)$ is the output, $H(s)$ is the plant and $G(s)$ is the transfer function of the PI controller [Ozyetkin et al., 2018].

Replacing:

$$\frac{I_{d_i}}{I_{d_i(\text{ref})}} = \frac{sK_{pi} + K_{iI}}{s^2L + s(R + K_{pi}) + K_{iI}}, \tag{2.16}$$

a classical second order equation can represent the denominator of the inner loop transfer function.

$$s^2 + s\left(\frac{R + K_{pi}}{L}\right) + \frac{K_{iI}}{L} = 0 = s^2 + 2\xi\omega_n s + \omega_n^2, \tag{2.17}$$

finding the constants:

$$K_{pi} = 2\xi\omega_n L - R, \qquad K_{iI} = \omega_n^2 L. \tag{2.18}$$

There are several forms to tune K_{pi} and K_{iI}, considering the best impulse response of the internal loop, the tuning that has a steady state error (ε), and settling time(t_s) is chosen.

$$\omega_n = -\frac{\ln(\varepsilon)}{\xi t_s}. \tag{2.19}$$

Knowing the state-space representation for the inner Loop control the following equations are found

$$L_{\text{grid}_1}\dot{x}_3 = (I_{d1(\text{ref})} - x_3)K_{pi} + K_{iI}x_4 + V_{\text{grid}} - x_3 R_{\text{grid}},$$
$$\dot{x}_4 = I_{d1(\text{ref})} - x_3,$$

where $x_3 = I_{d1}$ and x_4 is the integral action of the inner loop.

2.1.6 Outer Loop

The outer loop is necessary to control the DC voltage of the load, the voltage regulation can be solved by an outer loop with a PI control action, with the following transfer function:

$$PI(s) = K_{po} + \frac{K_{io}}{s}. \tag{2.20}$$

Considering (2.15) the transfer function in Figure 2.7 is represented in Laplace domain.

$$\frac{I_{d_i(\text{ref})}}{V_{DC_i(\text{ref})}} = \frac{sK_{po} + K_{io}}{s^2 L + s\frac{K_{po}}{C} + \frac{K_{io}}{C}}, \tag{2.21}$$

representing the denominator of the outer loop as a classical second order equation:

$$s^2 L + \frac{K_{po}}{C}s + \frac{K_{io}}{C} = 0 = s^2 + 2\xi\omega_n s + \omega_n^2, \tag{2.22}$$

by comparing , we get:

$$K_{po} = 2\xi\omega_n C, \qquad K_{io} = \omega_n^2 C. \tag{2.23}$$

To tune the constants as in the case of the inner loop, the tuning with overshoot (M_p) is selected [Ogata, 2003].

$$M_p = \exp\left(\frac{\Pi\xi}{\sqrt{1-\xi^2}}\right), \tag{2.24}$$

where

$$\xi = \sqrt{\frac{\ln^2(M_p)}{\ln^2(M_p) + \Pi}}; \quad 0 \leq M_p \leq 1. \tag{2.25}$$

The new values of the constants K_{po} and K_{io} can be implemented in the simulations results.
On the other hand, the outer loop maintains the voltage in the dc link implementing the control block of the Figure 2.7.

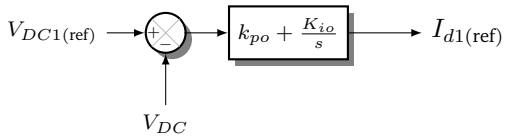

Figure 2.7: Control block diagram for the Outer Loop.

Applying the space of state representation for the outer loop control the following equations are found:

$$I_{d1(\text{ref})} = (V_{DC1(\text{ref})} - x_1)K_{po} + K_{io}x_5,$$
$$\dot{x}_5 = V_{DC1(\text{ref})} - x_1,$$

where x_5 is the integral action of the outer loop.

2.1.7 Power-sharing

The DC voltage droop control is implemented to ensure accurate sharing of load power. The active power-sharing is achieved by controlling voltage setpoints. However, AC systems nodes can be classified in PQ and PV (two variables) according to the control in each node, and DC systems nodes are controlled only for one variable [Park et al., 2018]. In AC droop control the closest resembling droop is the real (P-f) and reactive (Q-V) while DC microgrids only required (P-V) droop, avoiding the reactive power compensation, and reactive currents in the structure. Moreover, the control strategies simplified the synchronization with DC microgrids to the grid since the elimination of frequency and voltage phase angles [Alabdulwahab and Shahidehpour, 2016]. The DC voltage droop is shown in Figure 2.8.

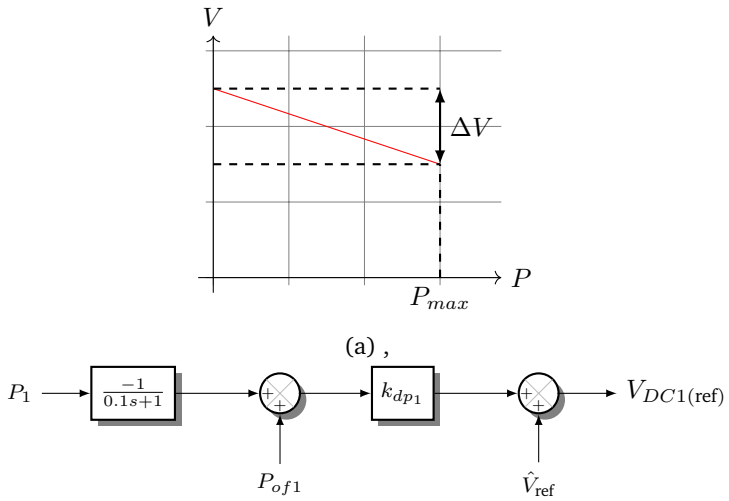

Figure 2.8: P-V droop control in DC: (a) P-V droop characteristic in DC micro-grids and (b) Control block diagram for the droop control .

From Figure 2.8, P_1 is the power grid at the point of common coupling, P_{of1} is the desired reference power, k_{dp_1} is the droop constant.

$$\dot{x}_6 = 10(P_{of1} - x_6),$$
$$P_1 = V_{\text{grid}} x_3,$$

where x_6 is the power of the droop control.

The equations for two converter-based DC micro-grid are described, and the steady-state model can be developed for n converters.

2.2 Complete dynamical model

The behavior of the dynamics of the system may be described by a set of n first-order differential equations.

$$\dot{x_i} = A_l x_n + \varphi(x_n) + Bu \qquad i = 1, 2, \ldots, n. \tag{2.26}$$

where x is the state vector of the system with n dimension, u is the input vector with m dimension, $A_l \in \mathbb{R}^{n \times n}$ represents the linear inputs, φ is no-linear inputs and $B \in \mathbb{R}^{m \times n}$ represents the linear outputs.

Consequently, the overall DC microgrid system can be written compactly for all nodes applying:

n is equal to $6k+1$ and is the length of the matrix A.
k is the number of the converters.
s is equal to $6k-1$.
m is the length of the matrix B.
h is equal to $3k-1$.

$$C_{DC_k}\dot{x}_{(1+s)} = \frac{V_{\text{grid}} - x_{(3+s)}}{x_{(1+s)}} - x_{(2+s)}. \tag{2.27}$$

$$L_{DC_k}\dot{x}_{(2+s)} = x_{(1+s)} - R_{DC_k}x_{(2+s)} - x_{(6n+1)}. \tag{2.28}$$

$$\begin{aligned} L_{\text{grid}_k}\dot{x}_{(3+s)} = {} & V_{\text{grid}(1+h)} - R_{\text{grid}_k}x_{(3+s)} + K_{pi_k}(K_{po_k}(\hat{V}_{\text{ref}(1+h)}, \\ & + K_{dp_k}(P_{of1(1+h)} - x_{(6+s)}) - x_{(1+s)}) + K_{io_k}x_{(5+s)}, \\ & - x_{(3+s)}) + K_{iI_k}x_{(4+s)}. \end{aligned} \tag{2.29}$$

$$\begin{aligned} \dot{x}_{(4+s)} = {} & K_{po_k}(\hat{V}_{\text{ref}(1+h)} + K_{dp_k}(P_{of1(1+h)} - x_{(6+s)}) - x_{(1+s)}), \\ & + K_{io_k}x_{(5+s)} - x_{(3+s)}. \end{aligned} \tag{2.30}$$

$$\dot{x}_{(5+s)} = \hat{V}_{\text{ref}(1+h)} + K_{dp_k}(P_{of1(1+h)} - x_{(6+s)}) - x_{(1+s)}. \tag{2.31}$$

$$\dot{x}_{(6+s)} = 10(V_{\text{grid}}x_{(3+s)} - x_{(6+s)}). \tag{2.32}$$

$$C_c\dot{x}_{(6n+1)} = \left(\sum_{k=1}^{n} x_{(2+s)}\right) - \frac{x_{(6n+1)}}{R_c}. \tag{2.33}$$

2.3 Results

Based on the equations for the design of the control system explained above, the formulas for two converters are formulated by calculating the constants K_{pi}, K_{iI}, K_{po}, K_{io} and k_{droop} as follows.

Inner Loop

$$\begin{gathered} \varepsilon = 0.02,\ t_s = 1e^{-3},\ \xi = 4,\ \omega_n = 978.0058, \\ K_{pi} = 430.2725,\ \ K_{iI} = 5.2607e^{4}. \end{gathered} \tag{2.34}$$

Outer Loop

$$\begin{gathered} Mp = 0.05,\ \omega_n = 2\pi 60,\ \xi = 4.0702 \\ K_{po} = 6.7515,\ \ K_{io} = 625.3381. \end{gathered} \tag{2.35}$$

Power Control

$$K_{dp_1} = 0.025,\ \ K_{dp_2} = 0.025. \tag{2.36}$$

The parameters for DC microgrid applying (2.26) are expressed in Table 2.2 for the two converters.

Table 2.2: Parameters of DC microgrid for two converters.

Parameter	Value	Parameter	Value
R_{grid}	$50e^{-3}$	C_c	$500e^{-6}$
L_{grid}	$55e^{-3}$	R_c	100
C_{DC1}	$2200e^{-6}$	C_{DC2}	$2200e^{-6}$
R_{DC1}	0.2	R_{DC2}	0.2
L_{DC1}	$1e^{-3}$	L_{DC2}	$1e^{-3}$
P_{of1}	800	P_{of2}	800
V_{grid}	400	w_n	$2\pi 60$

Hence, the state-space matrix A has a dimension of 13×13.

$$C_{DC_1}\dot{x}_1 = \frac{V_{\text{grid}} - x_3}{x_1} - x_2. \tag{2.37}$$

$$L_{DC_1}\dot{x}_2 = x_1 - R_{DC_1}x_2 - x_{13}. \tag{2.38}$$

$$\begin{aligned} L_{\text{grid}_1}\dot{x}_3 = {} & V_{\text{grid}1_3} - R_{\text{grid}_1}x_3 + K_{pi_1}(K_{po_1}(\hat{V}_{\text{ref}1_2} + K_{dp_1}(P_{of1_1} - x_6) - x_1), \\ & + K_{io_1}x_5 - x_3) + K_{iI_1}x_4. \end{aligned} \tag{2.39}$$

$$\dot{x}_4 = K_{po_1}(\hat{V}_{\text{ref}1_2} + K_{dp_1}(P_{of1_1} - x_6) - x_1) + K_{io_2}x_5 - x_3. \tag{2.40}$$

$$\dot{x}_5 = \hat{V}_{\text{ref}1_2} + K_{dp_1}(P_{of1_1} - x_6) - x_1. \tag{2.41}$$

$$\dot{x}_6 = 10(V_{\text{grid}}x_3 - x_6). \tag{2.42}$$

$$C_{DC_2}\dot{x}_7 = \frac{V_{\text{grid}} - x_9}{x_7} - x_8. \tag{2.43}$$

$$L_{DC_2}\dot{x}_8 = x_7 - R_{DC_2}x_8 - x_{13}. \tag{2.44}$$

$$\begin{aligned} L_{\text{grid}_2}\dot{x}_9 = {} & V_{\text{grid}2_6} - R_{\text{grid}_2}x_9 + K_{pi_2}(K_{po_2}(\hat{V}_{\text{ref}2_5} + K_{dp_2}(P_{of2_4} - x_{12}) - x_7), \\ & + K_{io_2}x_{11} - x_9) + K_{Ii_2}x_{10}. \end{aligned} \tag{2.45}$$

$$\dot{x}_{10} = K_{po_2}(\hat{V}_{\text{ref}2_5} + K_{dp_2}(P_{of2_4} - x_{12}) - x_7) + K_{io_2}x_{11} - x_9. \tag{2.46}$$

$$\dot{x}_{11} = \hat{V}_{\text{ref}2_5} + K_{dp_2}(P_{of2_4} - x_{12}) - x_7. \tag{2.47}$$

$$\dot{x}_{12} = 10(V_{\text{grid}}x_9 - x_{12}). \tag{2.48}$$

$$C_c\dot{x}_{13} = x_2 + x_8 - \frac{x_{13}}{R_c}. \tag{2.49}$$

To ratify that the state-space representation is providing the correct information from the system. The simulation is compiled using blocks, as shown in Figure 2.9, for comparing the results from the equations.

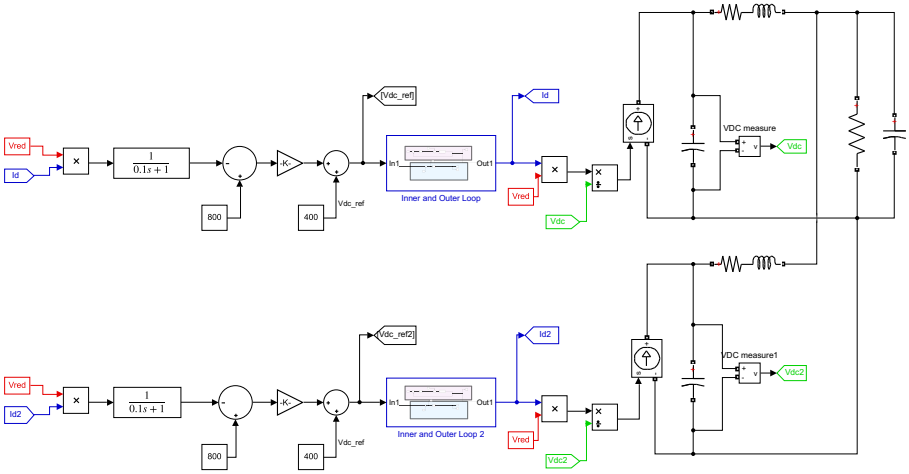

Figure 2.9: Simulation of the microgrid system by blocks.

2.4 Summary of results

In this chapter, the microgrid model with a single node was simulated by blocks and by state-space equations. For each model, the parameter was provided applying the formulas for the optimal control in Park and Clark frame references. Additionally, the mathematical model was designed with the inner and outer loop theory to guarantee the voltage and current regulation. Nevertheless, the power-sharing is required to ensure that the voltage setpoint is given a stable grid.

The state-space calculation was developed for n-converters. However, the simulations were modeled for two converters for simplifying the analysis. It was corroborated that the space-state model of the equation (2.26) is an appropriate representation of the microgrid model since the waveform of the grid current and DC voltage for both models is the same. The inner loop is controlling the power between the DC-link, and the grid. Indeed, the outer loop is controlling the DC voltage of the load. Thus, current and voltage are controlled efficiently following the reference since the DC voltage droop is controlling the voltage setpoint.

Comparing the results of the block simulation as is shown in Figure 2.9, with the state-space equations from (2.37) to (2.49), the variables are assigned. Where the $I_{d_{i_{mat_i}}}$ is the current for the state-space model simulated in Matlab, and the $I_{d_{i_{sim}}}$ simulated in Simulink by blocks. Similarly for the Figure 2.11, the $V_{DC_{i_{mat}}}$ represent the Matlab simulation, and $V_{DC_{i_{sim}}}$ for Simulink.

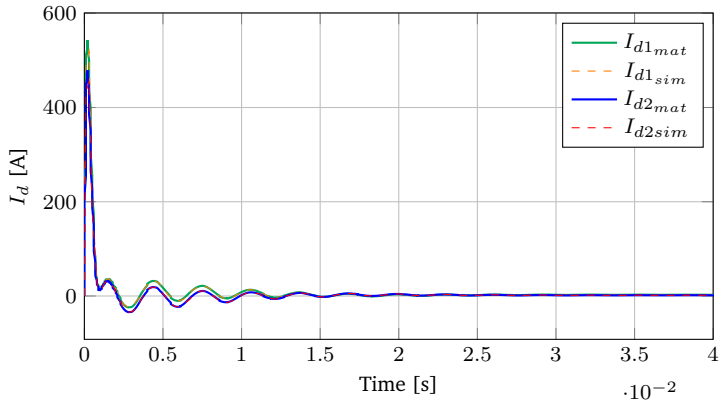

Figure 2.10: Grid current waveform for block simulation and state-space model.

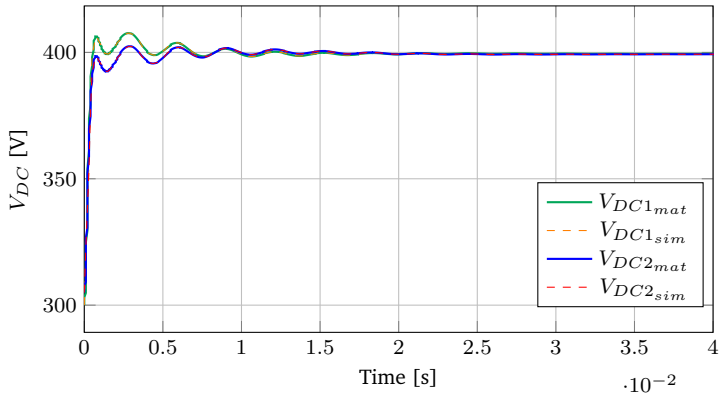

Figure 2.11: DC voltage waveform for block simulation and state-space model.

Figure 2.10 and 2.11 show the waveform of the grid current and DC link voltage. The response of the block simulation for the current is expressed by $Id_{i_{sim}}$, and state-space equations by $Id_{i_{mat}}$ for both converters. Evidencing that the tuning selected for the constants of the control is efficiently in the inner and control loop controllers. Also, the power-sharing sets the voltage in the specified value of $400\ V$.

Chapter 3

Small-signal analysis

The complexity and disturbances of the modern power system have increased, in the least years, because of the small variations in loads and generations. According to the stability theory, the system's stability can be understood depending on the duration of the fault that strongly influences on system stability and the ability to remain in synchronism. Stability Analysis is presented in two broad classes [Padiyar, 2008].

- Steady-State or Small-Signal Stability (SSS): It belongs to small disturbance.
- Transient Stability (TS): for a particular large disturbance or sequence of disturbances.

The study case of this research is small-signal stability (SSS) to analyze and control the dynamic stability of microgrid described in Section 2, maintaining synchronize the system. Physically power system stability can be classified into two main categories – angle stability or rotor angle stability and voltage stability [Mondal et al., 2014]. Voltage stability can be defined as "the ability of a system to maintain steady acceptable voltages at all buses following a system contingency or disturbance," guarantee the system conditions to control the droop. For this chapter, it is necessary to make the linearization of the system, allowing the analysis of eigenvalues and modes of oscillations.

3.1 Small-Signal stability

The small-signal study allows carrying out the analysis of the DC microgrids' stability under small disturbances. When the oscillations generated by the small disturbances are low for a long time, the DC microgrids will not present problems; therefore, it will be stable. Otherwise, DC microgrid will be unstable if the magnitude of the oscillations continues to increase [Garcés, 2018]. The operation of the DC microgrid can be affected by small disturbances that are

generated by numerous factors, characteristics of the control devices, initial operating conditions, the components of the DC microgrid, etc.

The small-signal dynamics of a DC microgrid are obtained by linearizing its dynamic systems around a steady-state operating point [Mondal et al., 2014]. The initial condition is normally computed from a base case's power flow solution, which can be calculated using the classical Newton's method. Furthermore, Newton's method guarantees the solution with a globally convergent property, if it exists regardless of its initial point [Eajal et al., 2016]. According to Newton's method, the set of nonlinear equations modeling the steady-state behavior, when iteratively the linearizations of the system get closer to the steady-state operating point as

$$\begin{aligned} \min \quad & f_i(x_1, \ldots, x_n), && (3.1)\\ & A(x_1, \ldots, x_n) = b, && (3.2)\\ & && (3.3) \end{aligned}$$

Using the Lagrangian representation the model can be written as (3.4).

$$\min \quad \mathcal{L}(x_1, \ldots, x_n, \lambda_1, \ldots, \lambda_n) = f_i(x_1, \ldots, x_n) + \lambda^\top (Ax_n - b). \tag{3.4}$$

where

$$f_i(x) = \frac{\partial \lambda}{\partial x} = \frac{\partial f}{\partial x} + A^\top \lambda = 0, \tag{3.5}$$

$f_i(x_n)$ is the set of non linear equation, $\mathcal{N} = (1, 2, \ldots n)$ are the variables assigned as x_n and $Df_i(x_n)$ is the Jacobian for the functions $f_i(x_n)$. The update is represented by Δ^k that assures $f_i(x_k + \delta k) < f_i(x_k)$ as follow.

$$\Delta f_i(x_n^k) = f_i(x_n) - f_i(x_n^k) = Df_i(x_n^k)\Delta x_n^k, \tag{3.6}$$

$$\Delta x_n^k = [Df_i(x_n^k)]^{-1} \Delta f_i(x_n^k), \tag{3.7}$$

The steady-state operating point is represented in (3.8).

$$x_n^{(k+1)} = x_n^k - [Df_i(x_n^k)]^{-1} \Delta f_i(x_n^k). \tag{3.8}$$

3.1.1 Linearization

Linearization is a linear approximation of a nonlinear system that is valid in a small region around an operating point. Considering that a nonlinear system can be defined as

$$\dot{x} = f(x) + g(x)u, \tag{3.9}$$

where $x \in \mathbf{R}^n$ is the states vector, $g(x) \in \mathbf{R}^{n\times m}$ is the input matrix, and $u \in \mathbf{R}^m$ is input control.

Let A denotes the Jacobian matrix of system (3.9) with respect to x whose elements are given by partial derivatives $\partial f_i/\partial x_n$ around a steady-state operating point, while B denotes the Jacobian matrix of system (3.9) with respect to u at the same point.

$$A = \frac{\partial}{\partial x}\left(f(x) + g(x)u\right)\Big|_{(x_o,u_o)}, \tag{3.10}$$

$$B = \frac{\partial}{\partial u}\left(f(x) + g(x)u\right)\Big|_{(x_o,u_o)}, \tag{3.11}$$

where x_o and u_o represent the operating point for states variables and input control.

The linear approximation of the nonlinear system (3.9) can be represented as

$$\Delta\dot{x} = A\Delta x_n + B\Delta u. \tag{3.12}$$

$$A = A_l x + \varphi(x). \tag{3.13}$$

Now, applying the linear approximation to system dynamic (2.26), the matrices A and B have the following form,

$$A = \begin{pmatrix}
\frac{-V_{\text{grid}}x_{(3_0+s)}}{C_{DC_k}}\left(\frac{1}{x^2_{(1_0+s)}}\right) & \frac{-1}{C_{DC_k}} & \frac{V_{\text{grid}}}{x_{(1_0+s)}C_{DC_k}} & 0 & & \\
\frac{1}{L_{DC_k}} & \frac{-R_{DC_k}}{L_{DC_k}} & 0 & 0 & & \\
\frac{-K_{pi_k}K_{po_k}}{L_{\text{grid}_k}} & 0 & \frac{-K_{pi_k}-R_{\text{grid}_k}}{L_{\text{grid}_k}} & \frac{K_{iI_k}}{L_{\text{grid}_k}} & & \\
-K_{po_k} & 0 & -1 & 0 & & \\
-1 & 0 & 0 & 0 & & \\
0 & 0 & 10V_{\text{grid}} & 0 & & \\
0 & \frac{\sum_{k=1}^{n}1}{C_c} & 0 & 0 & & \\
 & & 0 & 0 & 0 & \\
 & & 0 & 0 & \frac{-1}{L_{DC_k}} & \\
 & & \frac{K_{pi_k}K_{io_k}}{L_{\text{grid}_k}} & \frac{-K_{pi_k}K_{po_k}K_{dp_k}}{L_{\text{grid}_k}} & 0 & \\
 & & K_{io_k} & -K_{po_k}K_{dp_k} & 0 & \\
 & & 0 & -K_{dp_k} & 0 & \\
 & & 0 & -1 & 0 & \\
 & & 0 & 0 & -\frac{1}{R_cC_c} &
\end{pmatrix}$$

$$B = \begin{pmatrix} 0 & 0 & 0 \\ 0 & 0 & 0 \\ \frac{K_{pi_k} K_{po_k} K_{dp_k}}{L_{\text{grid}_k}} & \frac{K_{pi_k} K_{po_k}}{L_{\text{grid}_k}} & \frac{1}{L_{\text{grid}_k}} \\ K_{po_k} K_{dp_k} & K_{po_k} & 0 \\ K_{dp_k} & 1 & \\ 0 & 0 & 0 \\ 0 & 0 & 0 \end{pmatrix}$$

$$\begin{pmatrix} \Delta\dot{x}_{(1+s)} \\ \Delta\dot{x}_{(2+s)} \\ \Delta\dot{x}_{(3+s)} \\ \Delta\dot{x}_{(4+s)} \\ \Delta\dot{x}_{(5+s)} \\ \Delta\dot{x}_{(6+s)} \\ \Delta\dot{x}_{(6n+1)} \end{pmatrix} = [A] \begin{pmatrix} \Delta x_{(1+s)} \\ \Delta x_{(2+s)} \\ \Delta x_{(3+s)} \\ \Delta x_{(4+s)} \\ \Delta x_{(5+s)} \\ \Delta x_{(6+s)} \\ \Delta x_{(6n+1)} \end{pmatrix} + [B] \begin{pmatrix} \Delta P_{of1(1+r)} \\ \Delta \hat{V}_{\text{ref}(1+r)} \\ \Delta V_{\text{grid}(1+r)} \end{pmatrix}$$

Based on the all equations are linear, state-space model can be written as

$$f_i(x_n) = Ax_n + Bu. \tag{3.14}$$

where
x_n is the state vector of the system with n dimension.
u is the input vector with m dimension.
A is the linear inputs matrix of size $n \times n$.
B is the linear outputs matrix of the plant of size $m \times n$.

The equilibrium point can be calculated numerically with:

$$f(x_0) = 0. \tag{3.15}$$

3.1.2 Stability analysis

The theoretical basis to study microgrids small-signal stability is the Lyapunov linearized method. Linear systems allow finding if a system is stable by identifying the eigenvalues and eigenvectors of state matrix A. According to this method, there are two behaviors for the small disturbance in steady-state; The first case is that the oscillations of all modes are decaying approaching zero with the time being asymptotically stable, thus, all eigenvalues of the corresponding matrix A have a negative real part. Another possibility is that oscillations increase indefinitely with the time, and for that at least one of the eigenvalues of A lie on the right half part of the complex plane [Wang et al., 2010] .

The eigenvalues are represented by the scalar parameters λ, but it is only an eigenvalue of the matrix $A \in \mathbb{R}^{n \times n}$ if exists an n-column vector $\phi \in \mathbb{R}^n$ different to zero to the equation

$$A\phi_i = \lambda_i \phi_i \qquad i = 1, 2, \ldots, n. \tag{3.16}$$

To determinate the eigenvalues of the matrix A the following equation may be considered:

$$(A - \lambda_i I)\phi_i = 0, \tag{3.17}$$

for a non-trivial solution

$$\det(A - \lambda I) = 0. \tag{3.18}$$

Each of the vectors ϕ_i of (3.19) is known as the right eigenvector associated with the eigenvalue λ_i. Similarly, the left eigenvector ψ_i is related with the eigenvalue λ_i [Kundur et al., 1994].

$$A\psi_i = \lambda_i \psi_i. \tag{3.19}$$

Hence, there is n eigenvalue for a nxn matrix, but the eigenvector is not unique generated by the following analysis. Where the left and right eigenvectors associating with different eigenvalues are orthogonal.

$$\Phi = [\Phi_1 \;\; \Phi_2 \;\; \ldots \;\; \Phi_n], \tag{3.20}$$

$$\Psi = [\Psi_1^\top \;\; \Psi_2^\top \;\; \ldots \;\; \Psi_n^\top]^\top, \tag{3.21}$$

$$\Lambda = \text{diag}(\lambda_i),$$

(3.19) can be expanded as shown (3.22).

$$A\Phi = \Phi\Lambda, \tag{3.22}$$

Thus,

$$\Phi A \Phi^{-1} = \Phi \Lambda \Phi^{-1}, \tag{3.23}$$

$$\Phi A \Phi^{-1} = \Lambda. \tag{3.24}$$

Applying eigen properties $\Psi\Phi = I$ and $\Psi = \Phi^{-1}$ is possible cancel the cross-coupling associated with the differential equation (3.12) with free motion.

$$\Delta \dot{x_i} = A \Delta x_n, \tag{3.25}$$

$$\Delta x_n = \Phi y_n, \tag{3.26}$$

$$\Delta \dot{x_i} = \dot{\Phi} y_i, \tag{3.27}$$

Then,

$$\Phi \dot{y_i} = A \Phi y_n, \tag{3.28}$$

$$\dot{y_i} = \Phi^{-1} A \Phi y_n, \tag{3.29}$$

$$\dot{y_i} = \Lambda y_n. \tag{3.30}$$

The new state equation is found with n uncoupled equations. The Figure 3.1 shows the trajectory behavior for the combinations of eigenvalues around the singular points, for the systems transformed in two dimensions.

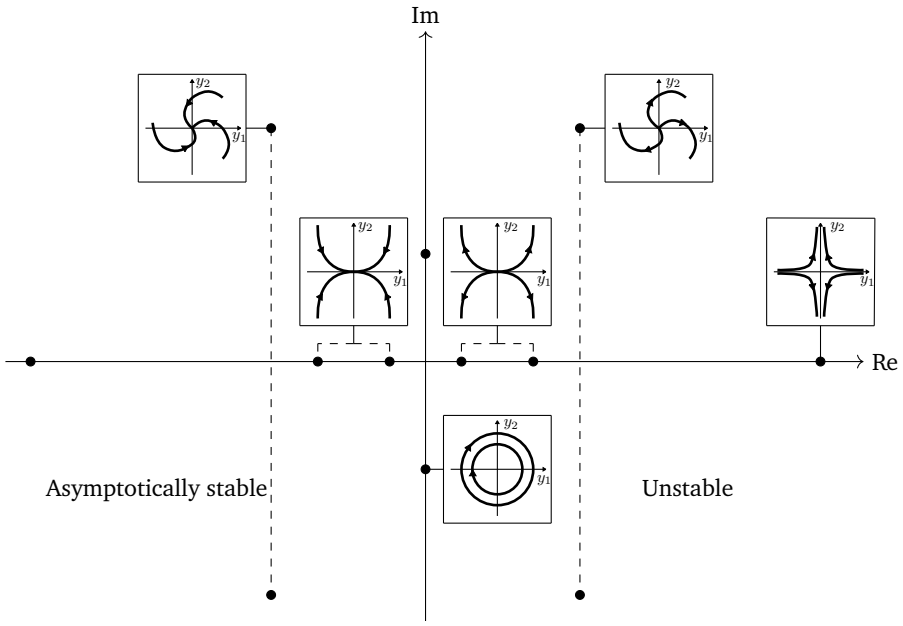

Figure 3.1: Trajectory behavior for the combinations of eigenvalues around the singular points

To clarify the stability analysis the transformation of (3.25) is given by

$$y(t) = y(0)e^{\lambda_i t}. \tag{3.31}$$

Such that $y(0)$ is the initial condition in t=0.

Therefore, system stability is determined by the eigenvalues λ_i and identified by time characteristic $e^{\lambda_i t}$. Complex eigenvalues have a conjugate pair ($\lambda = \sigma \pm j\omega$) where the real part of the eigenvalue describes system oscillation damping ξ and the imaginary part gives the frequency of oscillation.

$$\xi = \frac{-\sigma}{\sqrt{\sigma^2 + \omega^2}}. \tag{3.32}$$

As can be seen in the graphic the system is asymptotically stable if the real $\lambda_i < 0$ where the points that are on the imaginary axis produce a constant oscillation, consequently, they are considered stable.

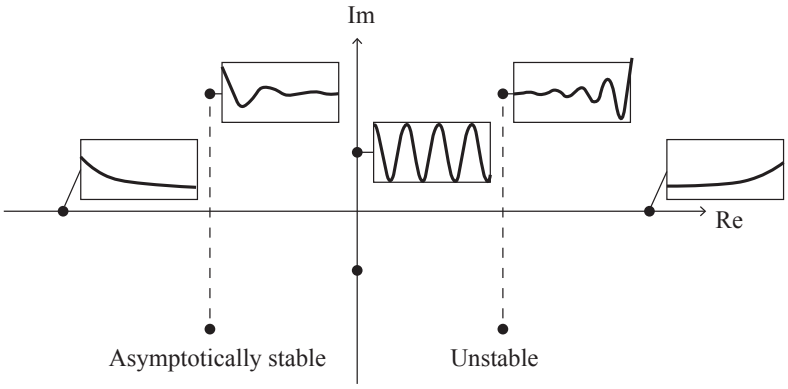

Figure 3.2: Trajectory of the dynamic system oscillation for the combinations of complex eigenvalues

3.1.3 Sensitivity analysis

To determine with state variables are more relational with the oscillations of the dynamical system, is required the sensitivity analysis of the eigenvalues considering (3.19).

$$A\phi_i = \lambda_i \phi_i \tag{3.33}$$

In order to establish the changes of the oscillations modes; the derivation is developed concerning parameter a_{km} of the matrix A.

$$\frac{\partial A}{\partial a_{km}}\phi_i + A\frac{\partial \phi_i}{\partial a_{km}} = \frac{\partial \lambda_i}{\partial a_{km}}\phi_i + \lambda_i \frac{\partial \phi_i}{\partial a_{km}} \tag{3.34}$$

Premultiplying by ψ_i:

$$\psi_i \frac{\partial A}{\partial a_{km}}\phi_i + \psi_i A\frac{\partial \phi_i}{\partial a_{km}} = \psi_i \frac{\partial \lambda_i}{\partial a_{km}}\phi_i + \psi_i \lambda_i \frac{\partial \phi_i}{\partial a_{km}} \tag{3.35}$$

$$\psi_i \frac{\partial A}{\partial a_{km}} = \psi_i \frac{\partial \lambda_i}{\partial a_{km}}\phi_i \tag{3.36}$$

Note that $\psi_i \phi_i = 1$ and $\partial \lambda_i / \partial a_{km}$ is a scalar, also $\partial A / \partial a_{km}$ is a matrix of zero with only one element in the km position which is equal to 1. Thus, the sensitivity is equal to the participation factor p_i^{km} of the respective states.

$$p_i^{km} = \frac{\partial \lambda_i}{\partial a_{km}} = \psi_i^k \phi_i^m \tag{3.37}$$

3.2 Results

Following the analysis of the small-signal dynamics is necessary to develop a load flow calculation at a given steady-state operation condition of the microgrid. Applying (3.5) the linearized equations are established. Thereafter, the resulting A system state matrix from (3.13) that was computed in Matlab, and its size will depend on the number of DC lines connected in the system. In this case, there are two connections to simplify the analysis of the results.

As explained previously in eigenvalues analysis all real parts must be negative to obtain an asymptotically stable system under all operational conditions. Therefore it is required to find the parameters which can achieve better stability in the system avoiding all the oscillations that cause the system to become unstable. The parameters that affect the behavior of the system most are the constant for the droop control, outer loop constants, inner loop constants, the filter resistance, and the filter inductance.

To demonstrate these variations; succeeding figures are showing the increase in the eigenvalues of the state matrix A, that is varying with respect to the base case. The dynamical system was simulated with the equilibrium point obtained in Table 3.1 from (3.8), applying the base case, by using Newton's method. The system is therefore stable asymptotically since the real part of each of the eigenvalues is negative, and the variable will reach to zero.

Table 3.1: Solution of the power flow (equilibrium point).

State variables	Value
x_1	400.0182
x_2	1.9981
x_3	2.1034
x_4	-0.0072
x_5	0.0034
x_6	799.2734
x_7	400.0182
x_8	1.9981
x_9	2.1034
x_{10}	-0.0072
x_{11}	0.0034
x_{12}	799.2734
x_{13}	399.6185

The equilibrium point is found when $f(x_0) = 0$, with the solution that is presented in the Table 3.2; it can be proved that Newton's method is a satisfactory technique to find the value with small error, as well as, the steady-state

equation is correctly modeling the system.

Table 3.2: Base case parameters and range evaluated for sensitivity analysis .

Parameter	Base case Value	Range evaluated
k_{droop}	0.025	400 x base
$K_{p\text{outer}}$	6.7515	29.6230 x base
$K_{i\text{outer}}$	625.3381	83.5548 x base
$K_{p\text{inner}}$	430.2725	2.3241 x base
$K_{i\text{inner}}$	$5.2607e^4$	100 x base
L_{grid}	$55e^-3$	100 x base
R_{grid}	$50e^-3$	360000 x base

A sensitivity analysis is required to identify which poles are more or less sensitive in the variation of the parameters or impact the system stability. To determine the stability of the microgrid for small variations around the equilibrium point; it is mandatory to compute the eigenvalues of the matrix A. The base case for the parameters that were previously shaded, appears in Table 3.2. Also, the range for generated different scenarios with the parameters on the stability analysis is given. The eigenvalues for the base case parameters have a real part, that achieved stability in the system. The real part of the eigenvalue defines how the magnitude of the parameters decreases or increases, while the imaginary part affects the frequency of oscillation.

Stability is a qualitative property of differential equations since it is not possible to affirm that one system is more or less stable than another. However, the greater the magnitude of the real part, the greater the rate of growth or decrease in the oscillation mode. Therefore, The damping rate can determine the oscillation mode. If it is less than 5%, as represented by the triangle for the eigenvalues graphics or square for damping variation images; may indicate oscillation problems that can be correct through proper parameters of the grid and controls [Mendoza-Armenta and Dobson, 2015].

3.3 Summary of results

The microgrid's small-signal stability was provided in this section, using the mathematical linearization model around a steady-state operating point, and applying Lyapunov theory. The process started with the analysis of the eigenvalues and modes of oscillations, for two converters. From Figure 3.3 to 3.16 the base case was varied to determinate which eigenvalues became unstable. Specifically, the value of the eigenvalues $K_{i\text{outer}}$ and L_{grid} in the last iterations; lies on the right half of the complex plane, thus the system is unstable for those scenarios.

The selection of the parameters of Table 3.2 can support the DC microgrid to be robust against different disturbances. Besides, damping ratio analysis improves the stability of the system, as is shown in the damping graphics. Where the axis x is the variation for each of the parameters, y represents the state variables and z the damping in percentage. If the damping is 100% for all variations, it is guaranteed that the constant is not affected by the state variable; since it will be asymptotically stable and should not be analyzed in all graphs. Instead, if the damping graphics are decaying below the blue square, as in Figure 3.8 and 3.14, evidence that those parameters have more impact in the stability.

Varying the parameter for the droop controller k_{droop} in a range between 0.025 and 10. The system of the Figure 3.3 becomes less stable but in minimal proportion as is evidence in Figure 3.4 where the oscillations are minor.

The control constant for $K_{p\text{outer}}$ and $K_{i\text{outer}}$ are presenting different behaviors, since Figure 3.5 is affected similarly with the droop coefficient. However, Figure 3.7 became unstable proving that the system is more sensible with considerable damping variations in Figure 3.8 associating with DC voltage, circuit current, AC current, and load voltage.

Analysing the eigenvalues for the inner lopp constants in Figure 3.9, 3.11, the system do not have important influence in the stability and, the oscillatory Figure 3.10, 3.12 becomes more stable and better damped with larger values.

The iteration of L_{grid} by the subtraction between DC voltage reference and DC voltage, and reference power affect the stability significantly. On the hand, Figure 3.15 for R_{grid} possess exponential functions or constant lines that do not affect stability. Clearly, the system is less oscillatory when the imaginary part is smaller, so it is damped out at a much faster rate.

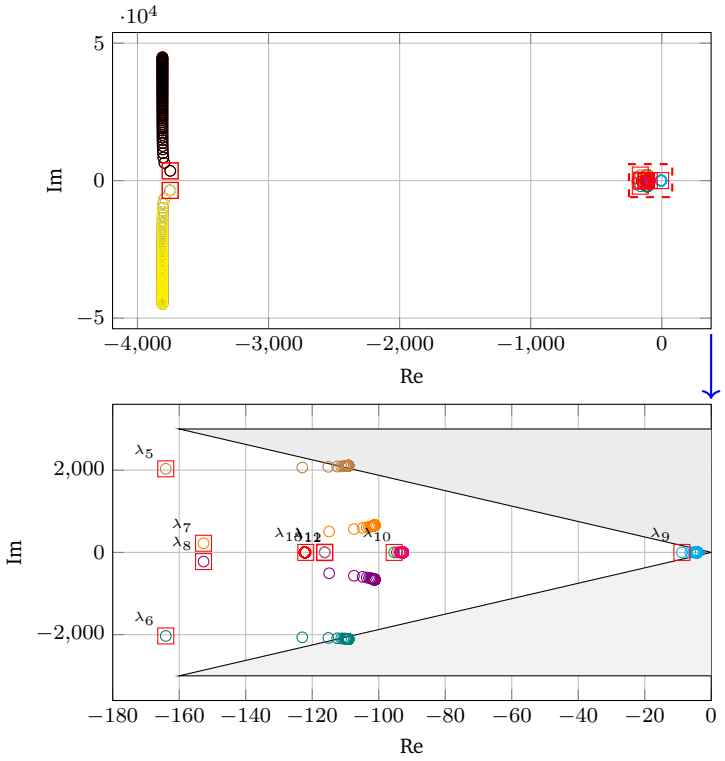

Figure 3.3: Eigenvalues of the system for different values of k_{droop}. The points marked with square represent the base case and the rest of the points are the variations of the eigenvalues as k_{droop} increases.

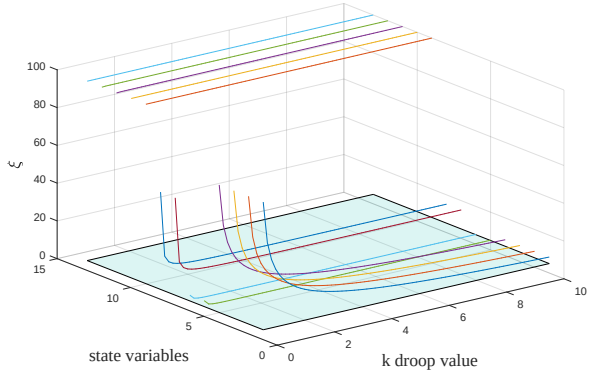

Figure 3.4: Damping variation for different values of k_{droop} .

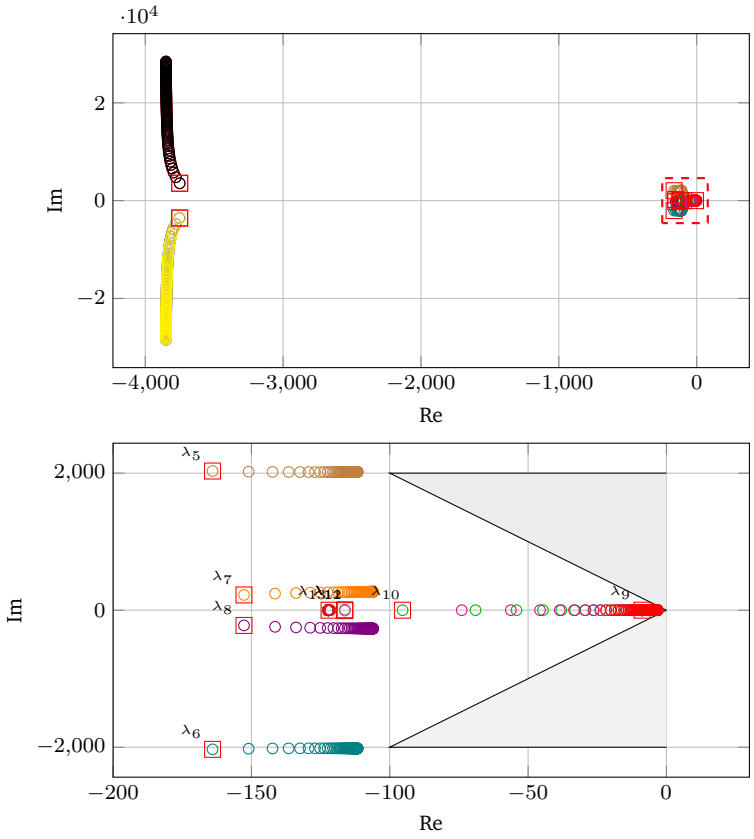

Figure 3.5: Eigenvalues of the system for different values of $K_{p\text{outer}}$. The points marked with square represent the base case and the rest of the points are the variations of the eigenvalues as $K_{p\text{outer}}$ increases.

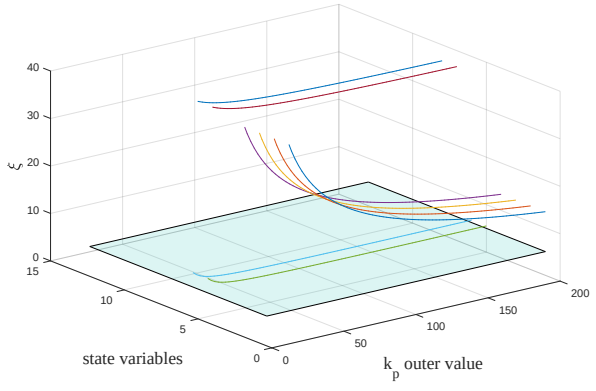

Figure 3.6: Damping variation for different values of $K_{p\text{outer}}$.

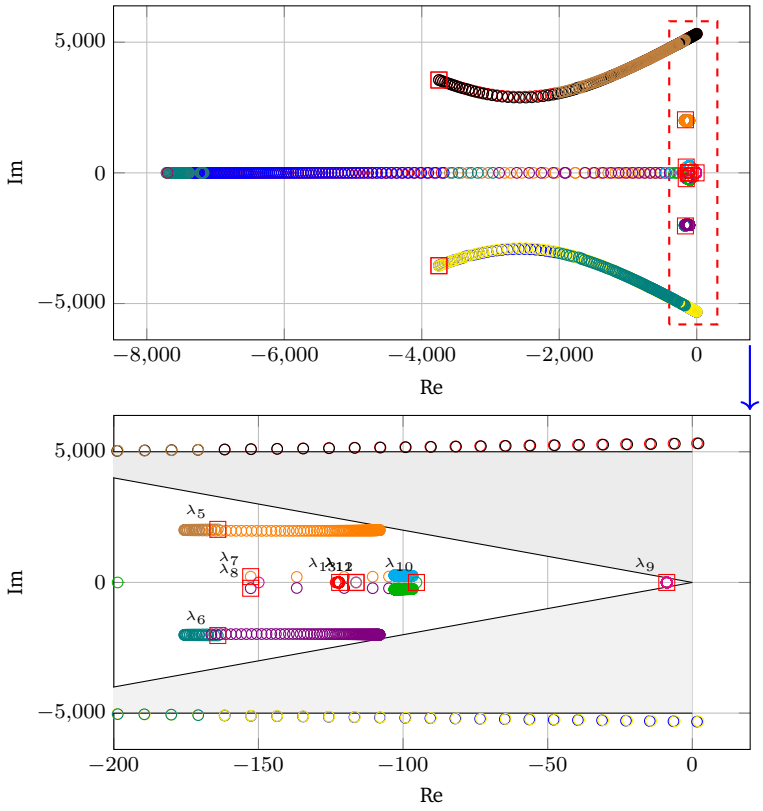

Figure 3.7: Eigenvalues of the system for different values of $K_{i\text{outer}}$. The points marked with square represent the base case and the rest of the points are the variations of the eigenvalues as $K_{i\text{outer}}$ increases.

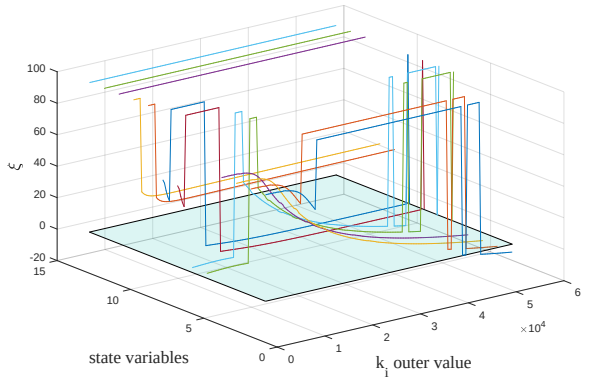

Figure 3.8: Damping variation for different values of $k_{i\text{outer}}$.

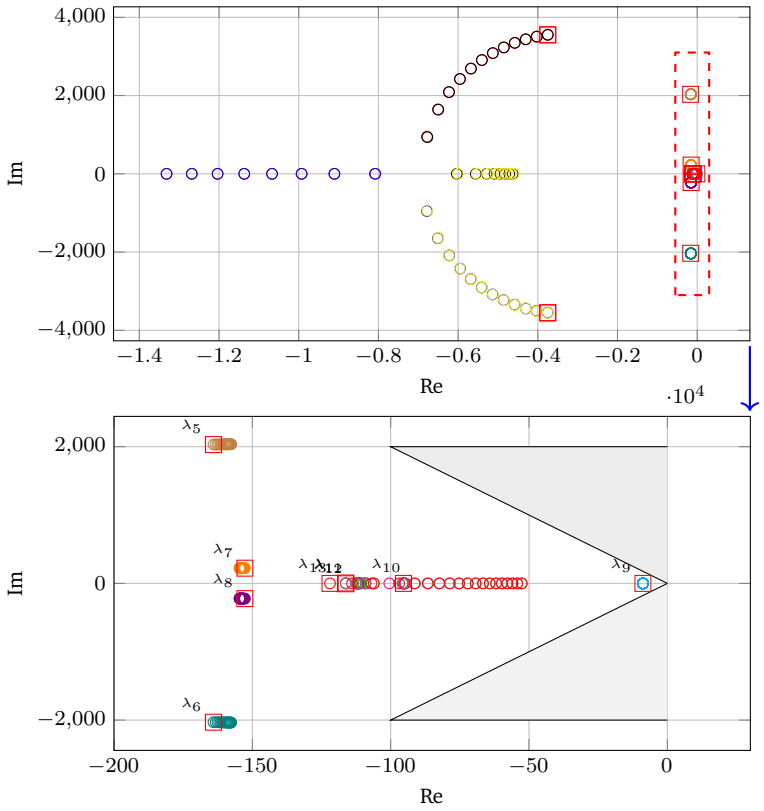

Figure 3.9: Eigenvalues of the system for different values of $K_{p\text{inner}}$. The points marked with square represent the base case and the rest of the points are the variations of the eigenvalues as $K_{p\text{inner}}$ increases.

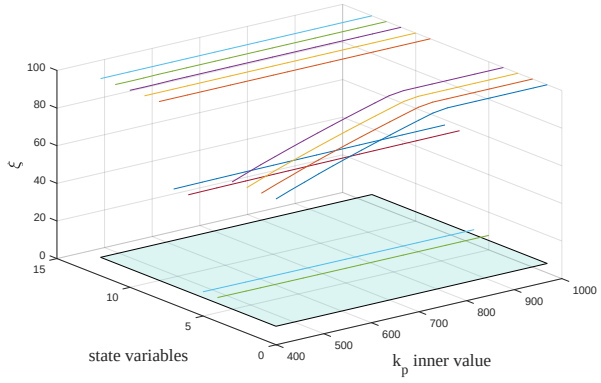

Figure 3.10: Damping variation for different values of $K_{p\text{inner}}$.

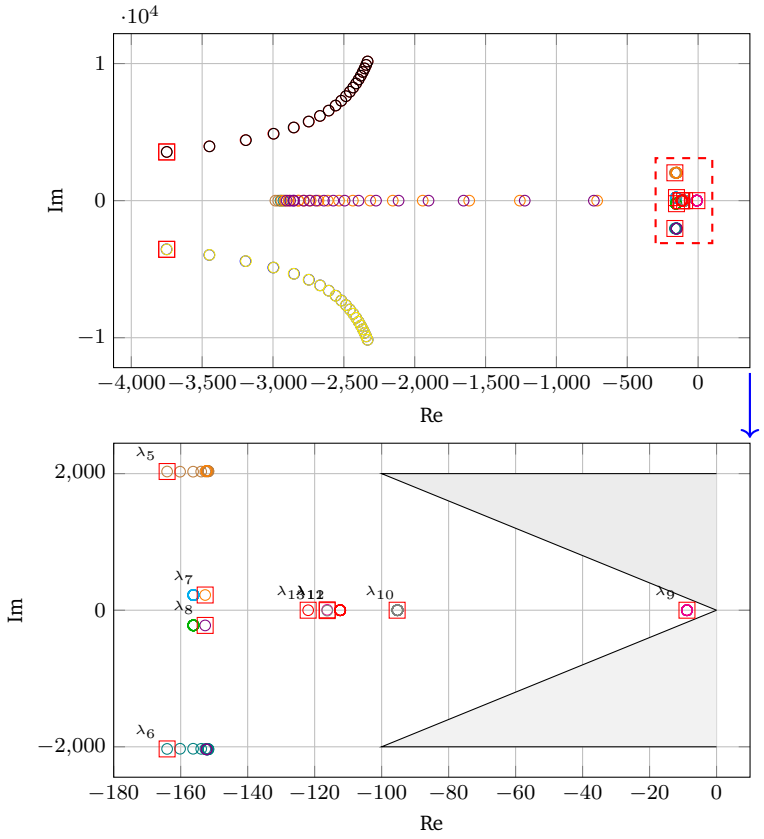

Figure 3.11: Eigenvalues of the system for different values of $K_{i\text{inner}}$. The points marked with square represent the base case and the rest of the points are the variations of the eigenvalues as $K_{i\text{inner}}$ increases.

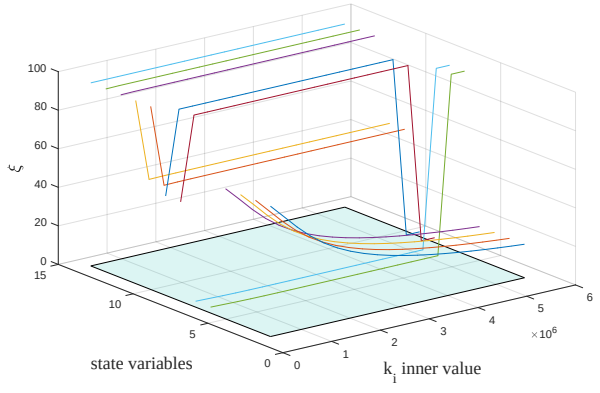

Figure 3.12: Damping variation for different values of $K_{i\text{inner}}$.

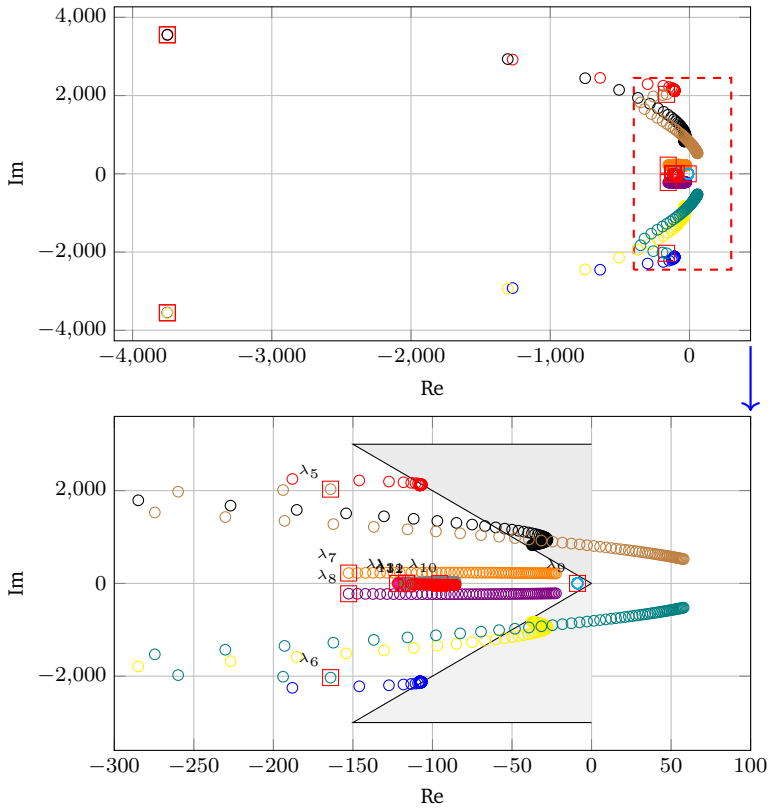

Figure 3.13: Eigenvalues of the system for different values of L_{grid}. The points marked with square represent the base case and the rest of the points are the variations of the eigenvalues as L_{grid} increases.

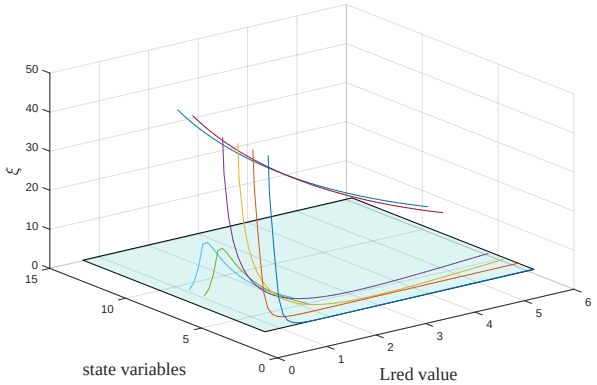

Figure 3.14: Damping variation for different values of L_{grid} .

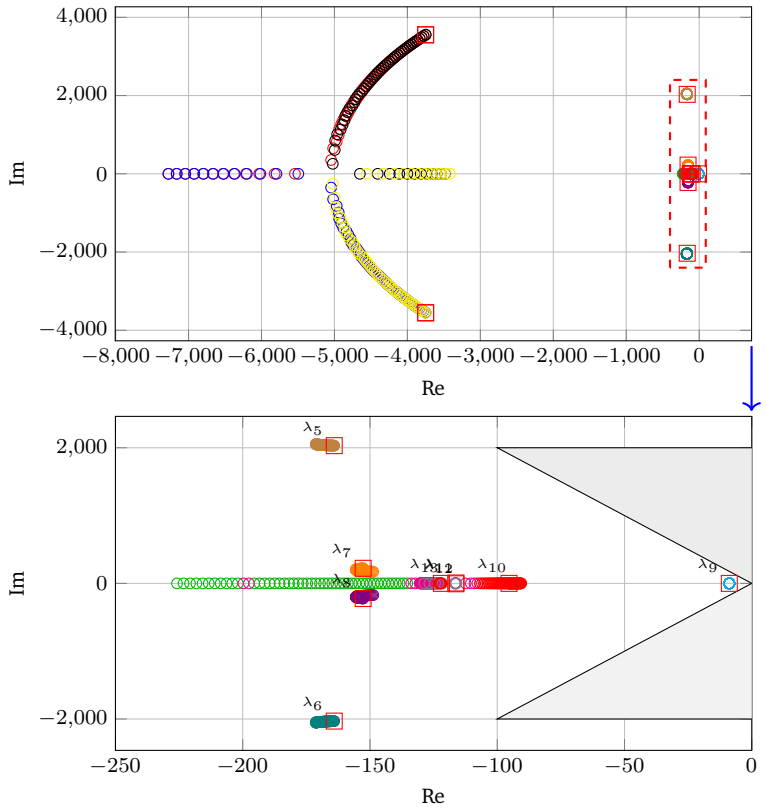

Figure 3.15: Eigenvalues of the system for different values of R_{grid}. The points marked with square represent the base case and the rest of the points are the variations of the eigenvalues as R_{grid} increases.

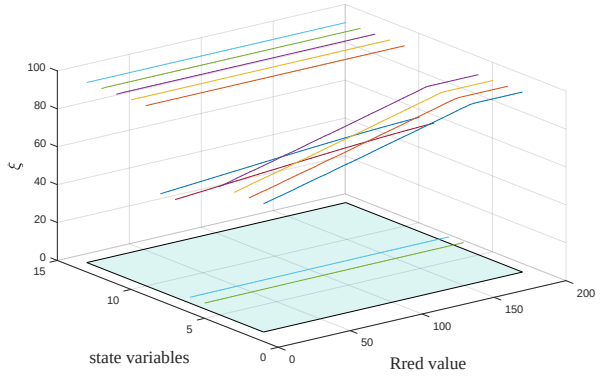

Figure 3.16: Damping variation for different values of R_{grid} .

The participation factor matrix from the right and left eigenvectors of the matrix A, for the base-case indicates the relationship between the states and the modes. As seen in Figure 3.17, the microgrid states have a dominant effect on the complex pair $\lambda_{4,13}$, $\lambda_{5,10}$, $\lambda_{5,11}$, $\lambda_{5,12}$, $\lambda_{10,10}$, $\lambda_{11,10}$, $\lambda_{11,10}$, $\lambda_{11,11}$, $\lambda_{11,12}$, $\lambda_{13,4}$, $\lambda_{13,5}$, $\lambda_{13,6}$; which represent the inner loop, outer loop and DC circuit in both converters.

Base-case ensures stable operation improving the stability of the DC microgrid according to correctly steady-stead performance. Moreover, the influence of control constants is satisfactory to the damping results of these oscillations modes.

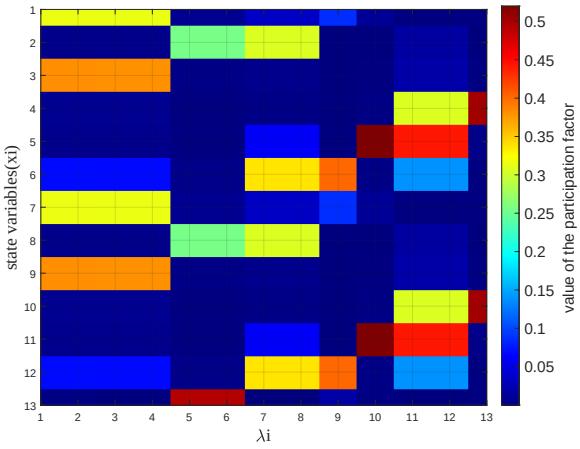

Figure 3.17: Representation of the matrix of the participation factors of the base case.

Chapter 4

Optimization Problem

The main aim of this chapter is to formulate a robust problem for different operation states of the DC microgrid. It is required to proving a comprehensive study on the application of convex optimization by formulating linear matrix inequalities (LMIs), as the constraints of the optimization problem in the semidefinite program (SDP) form, and solve using cvx. The SDPs structure has the advantage that allows robust control for minimizing the oscillations problems in the DC microgrid. Moreover, the Lyapunov function is found using convex techniques by adding an artificial variable as the objective of the problem.

4.1 Convex Optimization

To design the model of optimization is the essential clasify the four different types of mathematical optimization problems: linear programming (LP), integer programming (IP), nonlinear programming (NLP), and mixed-integer nonlinear programming(MINLP). Linear functions predominate in mathematical programming, for their convenient mathematical properties. The importance of those functions is attached to convex spaces since it is related to considerable advantages. In brief, a convex model guarantee uniqueness in the solution and convergence under specific conditions, also global optimum and real-time operation, since any convex problem can be computationally solved.

Integer problems as well as most non-linear problems are non-convex and therefore do not guarantee global optimum. However, there are several methodologies to convert into convex approximations. The theoretical foundation of convex optimization and its application range allows guaranteeing efficient results for each of the different types of applications. Specifically, convex optimization problems are those that are defined within a space of convex solutions. The convex spaces can be identified graphically, with Figure 4.1, which shows a convex set Ω_A and a non-convex set Ω_B. The first set is convex since the points

in the line segment $[x_1, x_2]$ are not out of space. The formal definition is presented below:

Convex optimization problems, $\Omega \subseteq \mathbb{R}^n$ can be identified by any pair of points, x_1,$x_2 \in \Omega$, one has $[x_1, x_2] \subseteq \Omega$ where $[x_1, x_2]$ is the line segment connecting x_1 and x_2 such that

$$(1 - \lambda)x_1 + \lambda x_2 \in \Omega. \tag{4.1}$$

For all $\lambda \in \mathbb{R}, 0 \leq \lambda \leq 1$.

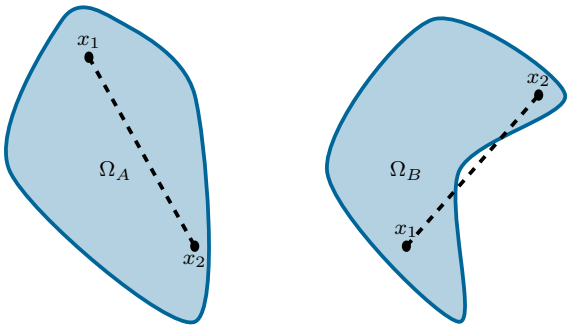

Figure 4.1: Example of a convex Ω_A and a non-convex Ω_B sets. In a convex space, all points in the interval $[x_1, x_2]$ belong in the space.

A function $f : \mathbb{R}^n$ is convex if the domain is convex. This implies for all pair of points $A, B \in \mathbb{R}^n$ such that

$$f(\lambda x_A + (1 - \lambda)x_B) \leq \lambda f(x_A) + (1 - \lambda)f(x_B). \tag{4.2}$$

For all $\lambda \in \mathbb{R}, 0 \leq \lambda \leq 1$.

Figure 4.2 represents a convex and non-convex function, where any line segment between two points A,B must be above the function to make it convex.

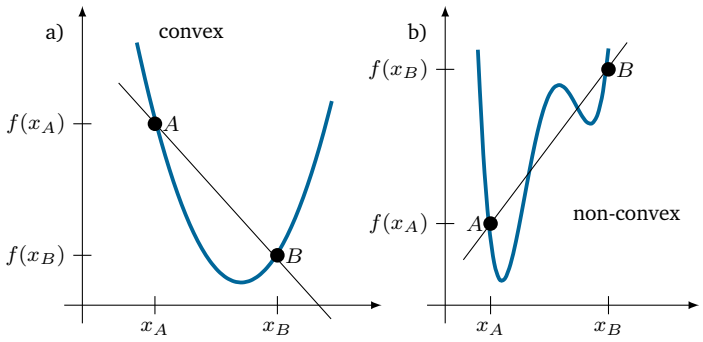

Figure 4.2: Example of a convex and a non-convex function. In a convex function, all points in the interval $[A, B]$ lies above the graph.

A convex optimization problem has the form [Boyd et al., 2004]

$$\begin{array}{ll} \text{min} & f_0(x) \\ \text{subject to} & f_i(x) \leq b_i, \quad i = 1, \ldots, m, \end{array} \tag{4.3}$$

Where the functions $f_0, \ldots, f_m : \mathbb{R}^n \to \mathbb{R}$ are convex and satisfy

$$f_i(\alpha x + \beta y) \leq \alpha f_i(x) + \beta f_i(y), \tag{4.4}$$

with

$$\alpha + \beta = 1 \quad \alpha \geq 0, \beta \geq 0. \tag{4.5}$$

A particular type of convex optimization models are formulated as generalized inequality constraints by applying the inequality constraint to be vector value, and employing generalized inequalities in the constraints [Boyd et al., 2004].

$$\begin{array}{ll} \text{min} & f_0(x) \\ \text{subject to} & f_i(x) \preceq K_i \, 0, \quad i = 1, \ldots, m \\ & Ax = b, \end{array} \tag{4.6}$$

where $f_0 : \mathbb{R}^n \to \mathbb{R}$, $K_i \subseteq \mathbb{R}^{k_i}$ are proper cones.

The formulation of the generalized inequality constraints is greater with cone problems, that posses a linear objective. The principal is to find the best geometric features that meet the objectives of the model. Thus, the hierarchy for some convex optimization is shown in Figure 4.3.

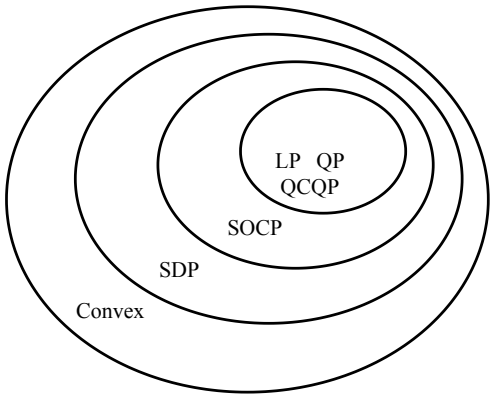

Figure 4.3: Hierarchy of several optimization problems.Semidefinite program (SDP), second-order cone program (SOCP), quadratic program (QP), quadratically constrained quadratic program(QCQP), Linear program LP.

This master's thesis is oriented to the use of semidefinite programming as presented in the next section.

4.2 Semidefinite programming

A particular case of conical optimization is the cone of positive semidefinite matrices, and the resulting problem is called SDP [Anjos and Lasserre, 2011]. Where a linear function of a symmetric matrix variable x is optimized subject to linear constraints on the elements of x, and additionals with x positive semidefinite. The inequality is modified, thus, k is the partial order induced on S^k by the cone of positive semidefinite $k \times k$ matrices, as follows

$$\begin{array}{ll} \text{min} & c^\top x \\ \text{subject to} & x_1 F_1 + \ldots + x_n F_n + G \preceq 0 \\ & Ax = b, \end{array} \tag{4.7}$$

where $c \in \mathbb{R}^m$ and $m+1$ symmetric matrices G, $F_1, \ldots, F_n \in S^k$, and $A \in \mathbb{R}^{p \times p}$.

Semidefinite programs unify several standard problems such as LP and QP, that in the majority of the cases the constraints are equivalent to linear matrix inequality (LMI) [Vandenberghe and Boyd, 1996]. Additionally, SDP appears in various important applications, and it can be solved efficiently in practice.

4.2.1 Linear matrix inequalities

LMIs arise in system and control theory, it can be formulated as convex optimization problems, and has the form

$$F(x) \triangleq F_0 + \sum_{i=1}^{m} x_i F_i \geq 0, \tag{4.8}$$

thus $x \in \mathbb{R}$ and the symmetric matrix $F_i = F_i^\top \in \mathbb{R}$, $i = 0, \ldots, m$, being $F(x)$ semi-defined positive, i.e. $u^\top F(x) u \geq 0$ for any number other than zero $u \in \mathbb{R}$.

Equation (4.8) is a convex constraint in x, as the set $\{x | F(x) > 0\}$ is convex. Although the shape of the LMI appears to be specified, due to (4.8), it can be represented by a diversity of convex constraints in x such as linear inequalities, quadratic inequalities, matrix norm inequalities, and constraints that arise in control theory such as Lyapunov and convex quadratic matrix inequalities [Boyd et al., 1994].

On the other hand, the Lyapunov theory can also be understood with the differential equation

$$\dot{x}(t) = Ax(t), \tag{4.9}$$

The system (4.9) is stable if and only if there exist a positive-define matrix Q such that

$$A^\top Q + QA < 0, \tag{4.10}$$

where $A \in \mathbb{R}^{n \times n}$ and $Q = Q^\top$ is the variable. In this case, LMIs is changed in a condensed form where $F_0 = 0$ and $F_i = -A^\top Q_i - Q_i A$.

Quadratic Lyapunov function can be found by solving the constraints $Q \geq 0$, $A^\top Q + QA \geq 0$ with any $I = I^\top \leq 0$ to solve the linear equation $A^\top Q + QA = -I$ for the matrix Q.

$$A^\top Q + QA + I \preceq 0, \tag{4.11}$$

Finally, the problem can be formulated as an optimization problem by adding an artificial variable μ

$$\begin{array}{ll} \text{max} & \mu \\ \text{subject to} & A^\top Q + QA \preceq -\mu I \\ & Q \geq 0 \\ & \mu \geq 0. \end{array} \tag{4.12}$$

If a Q exists, then Lyapunov function $V(z) = z^\top P z$ shows that the system $\dot{x}(t) = Ax(t)$ is globally asymptotically stable [Vandenberghe and Boyd, 1993].

4.3 Robust problem approach

The robust optimization techniques can be applied in the convex optimization problem as SDP in (4.12). Various scenarios are analyzed for different oper-

ating states, where the system is changing the percentage associated with the total power. The goal is to find a solution that is feasible for all data and optimal in some sense .

Formulating a robust approximation problems as SDPs, A is a matrix that has a variation $A = \{A_1, \ldots, A_k\}$. Resulting in several constraints that represent each of the scenarios.

$$\begin{array}{ll} \text{max} & \mu \\ \text{subject to} & A^\top(P_1)Q + QA(P_1) \preceq -\mu I \\ & A^\top(P_2)Q + QA(P_2) \preceq -\mu I \\ & A^\top(P_3)Q + QA(P_3) \preceq -\mu I \\ & \qquad \vdots \\ & A^\top(P_n)Q + QA(P_n) \preceq -\mu I \\ & Q \geq 0 \\ & \mu \geq 0. \end{array} \tag{4.13}$$

4.4 Results

To program the optimization problem in (4.12), the cvx software package is used to find the symmetric matrix Q that proves that the system is stable, and satisfy the inequality (4.11) for the SDP; when the constraints consist of LMI represented by Lyapunov inequality. Robust optimization permit to the DC microgrid more reliable results, since the converter power is varying in a range of percentages that simulate the five cases.

The different scenarios are proposed to the both converters of the test system found with (3.12). Figure 4.4 represent the power curves for the converter. The power for each converter is $800MW$ operating at 100% of the capacity, as is the case for the scenario P_{1_a} and P_{4_b}. For the first scenario the second converter power is $P_{1_b} = 80MW$, the second is $P_{2_a} = 320MW$ and $P_{2_b} = 560MW$ respectively, $P_{3_a} = 640MW$ and $P_{3_b} = 240MW$ in the third case. Finally $P_{5_a} = 480MW$ and $P_{5_b} = 400MW$ as is shown in Figure 4.4.

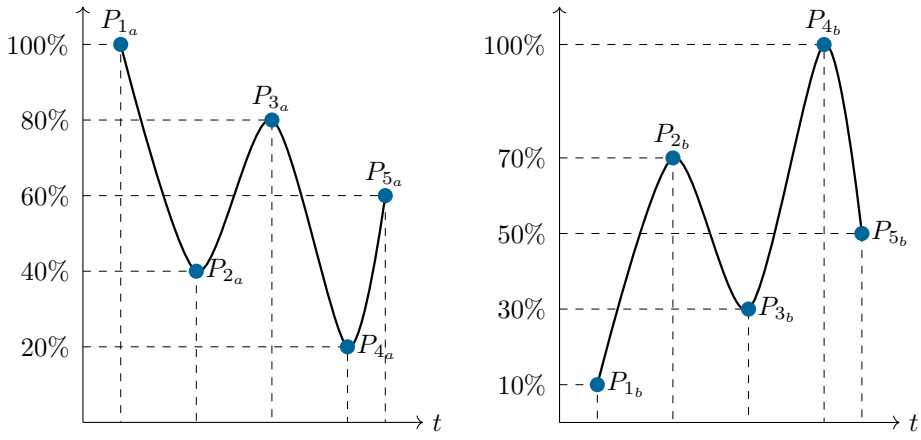

(a) Power for converter a.

(b) Power for converter b.

Figure 4.4: Power curves for both converters.

4.5 Summary of results

Convex optimization definition is necessary for applying semidefinite and robust programs described with emphasizing LMIs equations. In brief, The robust optimization evidenced the adequate operation of the control over the DC microgrid with the parameters of the base case implemented in chapter 3 that appear in Table 3.2. Generating a variation in the power for different scenarios of power states, as is shown in 4.4, the Lyapunov theory is demonstrated, since existing a matrix Q for the system.

It is necessary to define the variable A for the code, before the objective function that for this problem is the artificial variable μ, then the LMI constraints and the other constraints. cxv guarantee the result, with a solved status and optimal value of $1.0490e^{-14}$. The solver satisfies the constraints and finds the solution in only 26 iterations with a total time of 0.63 seconds. Hence, cvx is straightforward to implement.

$$Q = 1e^{7}\begin{pmatrix} 0.0452 & 0.0002 & 0.0000 & -0.0045 & 0.0946 & -0.0052 \\ 0.0002 & 0.0016 & 0.0000 & -0.0045 & -0.0242 & -0.0000 \\ 0.0000 & 0.0000 & 0.0000 & -0.0000 & -0.0001 & 0.0000 \\ -0.0045 & -0.0045 & -0.0000 & 0.2403 & 1.1308 & -0.0004 \\ 0.0946 & -0.0242 & -0.0001 & 1.1308 & 8.0218 & -0.0164 \\ -0.0052 & -0.0000 & 0.0000 & -0.0004 & -0.0164 & 0.0006 \\ 0.0446 & 0.0002 & 0.0000 & 0.0015 & 0.1260 & -0.0052 \\ 0.0002 & 0.0015 & 0.0000 & -0.0037 & -0.0202 & -0.0000 \\ 0.0000 & 0.0000 & 0.0000 & -0.0000 & -0.0000 & 0.0000 \\ 0.0015 & -0.0037 & -0.0000 & 0.0338 & 0.1575 & -0.0002 \\ 0.1260 & -0.0202 & -0.0000 & 0.1575 & 1.2406 & -0.0150 \\ -0.0052 & -0.0000 & 0.0000 & -0.0002 & -0.0150 & 0.0006 \\ 0.0096 & 0.0001 & -0.0000 & -0.0049 & 0.0026 & -0.0012 \end{pmatrix}$$

$$\begin{pmatrix} 0.0446 & 0.0002 & 0.0000 & 0.0015 & 0.1260 & -0.0052 & 0.0096 \\ 0.0002 & 0.0015 & 0.0000 & -0.0037 & -0.0202 & -0.0000 & 0.0001 \\ 0.0000 & 0.0000 & 0.0000 & -0.0000 & -0.0000 & 0.0000 & -0.0000 \\ 0.0015 & -0.0037 & -0.0000 & 0.0338 & 0.1575 & -0.0002 & -0.0049 \\ 0.1260 & -0.0202 & -0.0000 & 0.1575 & 1.2406 & -0.0150 & 0.0026 \\ 0.0052 & -0.0000 & 0.0000 & -0.0002 & -0.0150 & 0.0006 & -0.0012 \\ 0.0452 & 0.0002 & 0.0000 & -0.0045 & 0.0946 & -0.0052 & 0.0096 \\ 0.0002 & 0.0016 & 0.0000 & -0.0045 & -0.0243 & -0.0000 & 0.0001 \\ 0.0000 & 0.0000 & 0.0000 & -0.0000 & -0.0001 & 0.0000 & -0.0000 \\ -0.0045 & -0.0045 & -0.0000 & 0.2403 & 1.1308 & -0.0004 & -0.0049 \\ 0.0946 & -0.0243 & -0.0001 & 1.1308 & 8.0218 & -0.0164 & 0.0026 \\ -0.0052 & -0.0000 & 0.0000 & -0.0004 & -0.0164 & 0.0006 & -0.0012 \\ 0.0096 & 0.0001 & -0.0000 & -0.0049 & 0.0026 & -0.0012 & 0.0037 \end{pmatrix}$$

Chapter 5

Conclusions and future works

- An AC generator connected with a DC microgrid through VSC control has been designed. The performance has been found satisfactory under the control strategy, since both simulations, in the dynamic model and the block model, are stables and follow the references.
- The small-signal dynamics of a DC microgrid are obtained by linearizing its dynamic systems around a steady-state operating point with the Newton algorithm. However, Newton's method guarantees the solution with a globally convergent property, when existing regardless of its initial point.
- The theoretical basis to study microgrids small-signal stability is the Lyapunov linearized method. Allow finding if stable systems or unstable by identifying the eigenvalues and eigenvectors of state matrix A.
- The sensitivity analysis of the eigenvalues is required to determine with state variables are more relational with the oscillations of the dynamical system. Therefore, it is required to find the parameters which can achieve better stability in the system avoiding all the oscillations that cause the system to become unstable.
- The poles that have more impact on the variation of the parameters were identified, giving to the DC microgrid robustness against different disturbances and the influence of their ranges.
- Convex optimization allows formulated semidefinite problems with Lyapunov LMI as constraints. Also, the robust optimization guarantees that the system is asymptotically stable for various scenarios for the operating states when the solution is feasible and optimal for all data.
- The simulation of DC microgrid has been presented. The simulation is performed in the dynamical model and block model. The optimization effects are validated through several case studies under different operating conditions to find system identification with the optimum constants of the control.

5.1 Future works

The future works derived from this master's thesis are:

- Consider in the model Constant power loads (CPL), where exist uncertainty in the load.
- Develop a stability model considering the randomness of the primary resource.
- Employ bilinear matrix innequalities in convex optimization.

Bibliography

[Alabdulwahab and Shahidehpour, 2016] Alabdulwahab, A. and Shahidehpour, M. (2016). Microgrid networking for the monitoring, control and protection of modern power systems. *The Electricity Journal*, 29(10):1–7.

[Anjos and Lasserre, 2011] Anjos, M. F. and Lasserre, J. B. (2011). *Handbook on semidefinite, conic and polynomial optimization*, volume 166. Springer Science & Business Media.

[Blekherman et al., 2012] Blekherman, G., Parrilo, P. A., and Thomas, R. R. (2012). *Semidefinite optimization and convex algebraic geometry*. SIAM.

[Boyd et al., 2004] Boyd, S., Boyd, S. P., and Vandenberghe, L. (2004). *Convex optimization*. Cambridge university press.

[Boyd et al., 1994] Boyd, S., El Ghaoui, L., Feron, E., and Balakrishnan, V. (1994). *Linear matrix inequalities in system and control theory*, volume 15. Siam.

[Che et al., 2015] Che, L., Shahidehpour, M., Alabdulwahab, A., and Al-Turki, Y. (2015). Hierarchical coordination of a community microgrid with ac and dc microgrids. *IEEE Transactions on smart grid*, 6(6):3042–3051.

[Cominetti et al., 2012] Cominetti, R., Facchinei, F., and Lasserre, J. B. (2012). *Modern optimization modelling techniques*. Springer Science & Business Media.

[Dastgeer et al., 2019] Dastgeer, F., Gelani, H. E., Anees, H. M., Paracha, Z. J., and Kalam, A. (2019). Analyses of efficiency/energy-savings of dc power distribution systems/microgrids: Past, present and future. *International Journal of Electrical Power & Energy Systems*, 104:89–100.

[Diaz et al., 2015] Diaz, G. B., Suul, J. A., and D'Arco, S. (2015). Small-signal state-space modeling of modular multilevel converters for system stability analysis. In *2015 IEEE Energy Conversion Congress and Exposition (ECCE)*, pages 5822–5829. IEEE.

[dos Santos Neto et al., 2020] dos Santos Neto, P. J., Barros, T. A., Silveira, J. P., Ruppert Filho, E., Vasquez, J. C., and Guerrero, J. M. (2020). Power

management techniques for grid-connected dc microgrids: A comparative evaluation. *Applied Energy*, 269:115057.

[Eajal et al., 2016] Eajal, A. A., Abdelwahed, M. A., El-Saadany, E. F., and Ponnambalam, K. (2016). A unified approach to the power flow analysis of ac/dc hybrid microgrids. *IEEE Transactions on Sustainable Energy*, 7(3):1145–1158.

[Elsayed et al., 2015] Elsayed, A. T., Mohamed, A. A., and Mohammed, O. A. (2015). Dc microgrids and distribution systems: An overview. *Electric Power Systems Research*, 119:407–417.

[Garcés, 2018] Garcés, A. (2018). Small-signal stability analysis of dc microgrids considering electric vehicles. *Revista Facultad de Ingeniería Universidad de Antioquia*, (89):1–7.

[Garcés, 2019] Garcés, A. (2019). Stability analysis of dc-microgrids: A gradient formulation. *Journal of Control, Automation and Electrical Systems*, 30(6):985–993.

[Garces, 2020] Garces, A. (2020). Small-signal stability in island residential microgrids considering droop controls and multiple scenarios of generation. *Electric Power Systems Research*, 185:106371.

[Gil-González et al., 2020a] Gil-González, W., Garcés, A., and Fosso, O. B. (2020a). Passivity-based control for small hydro-power generation with pmsg and vsc. *IEEE Access*, 8:153001–153010.

[Gil-González et al., 2020b] Gil-González, W., Montoya, O. D., and Garces, A. (2020b). Modeling and control of a small hydro-power plant for a dc microgrid. *Electric Power Systems Research*, 180:106104.

[Kalitjuka, 2011] Kalitjuka, T. (2011). Control of voltage source converters for power system applications. Master's thesis, Institutt for elkraftteknikk.

[Kumar et al., 2017] Kumar, D., Zare, F., and Ghosh, A. (2017). Dc microgrid technology: system architectures, ac grid interfaces, grounding schemes, power quality, communication networks, applications, and standardizations aspects. *Ieee Access*, 5:12230–12256.

[Kundur et al., 1994] Kundur, P., Balu, N. J., and Lauby, M. G. (1994). *Power system stability and control*, volume 7. McGraw-hill New York.

[Liu et al., 2017] Liu, J., Zhang, W., and Rizzoni, G. (2017). Robust stability analysis of dc microgrids with constant power loads. *IEEE Transactions on Power Systems*, 33(1):851–860.

[Liu et al., 2015] Liu, S., Liu, P. X., and Wang, X. (2015). Stochastic small-signal stability analysis of grid-connected photovoltaic systems. *IEEE Transactions on Industrial Electronics*, 63(2):1027–1038.

[Manias, 2016] Manias, S. (2016). *Power electronics and motor drive systems*. Academic Press.

[Mendoza-Armenta and Dobson, 2015] Mendoza-Armenta, S. and Dobson, I. (2015). Applying a formula for generator redispatch to damp interarea oscillations using synchrophasors. *IEEE Transactions on Power Systems*, 31(4):3119–3128.

[Mondal et al., 2014] Mondal, D., Chakrabarti, A., and Sengupta, A. (2014). *Power system small signal stability analysis and control*. Academic Press is an imprint of Elsevier.

[Ogata, 2003] Ogata, K. (2003). *Ingeniería de control moderna*. Pearson Educación.

[Ozyetkin et al., 2018] Ozyetkin, M., Onat, C., and Tan, N. (2018). Pid tuning method for integrating processes having time delay and inverse response. *IFAC-PapersOnLine*, 51(4):274–279.

[Padiyar, 2008] Padiyar, K. (2008). *Power system dynamics: stability and control*. BS Publications.

[Park et al., 2018] Park, G.-C., Lee, W.-P., and Won, D.-J. (2018). Power sharing algorithm for voltage regulation in islanded dc multi-microgrid system. In *2018 53rd International Universities Power Engineering Conference (UPEC)*, pages 1–6. IEEE.

[Peng and Lai, 1996] Peng, F. Z. and Lai, J.-S. (1996). Generalized instantaneous reactive power theory for three-phase power systems. *IEEE transactions on instrumentation and measurement*, 45(1):293–297.

[Shakerighadi et al., 2018] Shakerighadi, B., Ebrahimzadeh, E., Blaabjerg, F., and Bak, C. L. (2018). Lyapunov-and eigenvalue-based stability assessment of the grid-connected voltage source converter. In *2018 IEEE International Power Electronics and Application Conference and Exposition (PEAC)*, pages 1–6. IEEE.

[Teodorescu et al., 2011] Teodorescu, R., Liserre, M., and Rodriguez, P. (2011). *Grid converters for photovoltaic and wind power systems*, volume 29. John Wiley & Sons.

[Vandenberghe and Boyd, 1993] Vandenberghe, L. and Boyd, S. (1993). A polynomial-time algorithm for determining quadratic lyapunov functions for nonlinear systems. Technical report, STANFORD UNIV CA INFORMATION SYSTEMS LAB.

[Vandenberghe and Boyd, 1996] Vandenberghe, L. and Boyd, S. (1996). Semidefinite programming. *SIAM review*, 38(1):49–95.

[Wang et al., 2020] Wang, Q., Yao, W., Fang, J., Ai, X., Wen, J., Yang, X., Xie, H., and Huang, X. (2020). Dynamic modeling and small signal stability analysis of distributed photovoltaic grid-connected system with large scale of panel level dc optimizers. *Applied Energy*, 259:114132.

[Wang et al., 2017] Wang, X., Harnefors, L., and Blaabjerg, F. (2017). Unified impedance model of grid-connected voltage-source converters. *IEEE Transactions on Power Electronics*, 33(2):1775–1787.

[Wang et al., 2010] Wang, X.-F., Song, Y., and Irving, M. (2010). *Modern power systems analysis*. Springer Science & Business Media.

[xm, 2020] xm (2020). En agosto, generación promedio diaria de energía fue de $188.7gwh$-día. `https://www.xm.com.co/Paginas/detalle-noticias.aspx?identificador=2971`.

[Yazdani and Iravani, 2010] Yazdani, A. and Iravani, R. (2010). *Voltage-sourced converters in power systems: modeling, control, and applications*. John Wiley & Sons.

[Zhang et al., 2013] Zhang, R., Li, Y., and Lou, Y. (2013). Convex optimization of battery energy storage station in a micro-grid. In *2013 IEEE International Conference on Information and Automation (ICIA)*, pages 1346–1351. IEEE.